Electron Beam Radiation Induced GMA-grafted Cotton Fibers Optimized with Phosphoric Acid for Adsorption of Metformin Hydrochloride from Aqueous Solution

Mohammed S. Alnaisani [a,*] Luqman Chuah Abdullah [b,*] Teo Ming Ting,[c] Siti Nurul Ain Md Jamil [d,e] Halimatun Sakdiah Zainuddin,[a] Mohammed Abdullah,[f] and Shihab Ezzuldin M. Saber [g]

Using an electron beam (EB) accelerator, natural cotton fibers were pre-irradiated for grafting with glycidyl methacrylate (GMA). Subsequently, phosphoric acid (phosphoric) was used to functionalize the GMA-grafted fibers (cotton-*g*-GMA). Various analyses, including scanning electron microscopy (SEM), Fourier transform infrared (FTIR) spectroscopy, X-ray diffraction (XRD), thermogravimetric and derivative thermogravimetric (TG-DTG) analysis, and surface charge analysis, were performed to evaluate the morphological and physiochemical attributes of the fibrous adsorbent. The prepared adsorbent was then tested for metformin hydrochloride (MFH) adsorption from an aqueous solution. The MFH's adsorption on phosphoric-cotton-*g*-GMA followed a pseudo-2nd order model. The Langmuir isotherm model was close behind the Redlich-Peterson model, which described the equilibrium data the best, according to the isotherm analysis. At 24.7 mg/g, the maximum adsorption capacity was attained. Meanwhile, the regeneration and recycling of the adsorbent were possible for at least five cycles, with recovery of MFH being nearly 94.65% in the final cycle. According to the findings, it was deduced that the fibrous phosphoric-cotton-*g*-GMA adsorbent could be used to successfully eliminate MFH at an industrial scale.

DOI: 10.15376/biores.21.1.2283-2314

Keywords: Radiation; Graft polymerization; Natural cotton fibers; Phosphoric acid functionalization; Metformin hydrochloride; Adsorption

*Contact information: a: Department of Chemical and Environmental Engineering, Faculty of Engineering, Universiti Putra Malaysia, UPM Serdang 43400, Selangor, Malaysia; b: Institute of Tropical Forestry and Forest Products (INTROP), Universiti Putra Malaysia, UPM Serdang 43400, Selangor, Malaysia; c: Radiation Technology Division, Malaysian Nuclear Agency, 43000, Kajang, Selangor, Malaysia; d: Department of Chemistry, Faculty of Science, Universiti Putra Malaysia, UPM Serdang 43400, Selangor, Malaysia; e: Centre of Foundation Studies for Agricultural Science, Universiti Putra Malaysia, UPM Serdang 43400, Selangor, Malaysia; f: Chemical Engineering Studies, College of Engineering, Universiti Teknologi Mara, Cawangan Johor, Kampus Pasir Gudang, 81750 Masai, Johor, Malaysia; g: North Refineries Company (NRC), Salahuddin, Iraq; *Corresponding author: chuah@upm.edu.my*

INTRODUCTION

Water is essential to all life on the planet and is especially vital to human survival. Because seawater makes up 97.5% of the total water volume on Earth, there is significantly less fresh water available (Khilchevskyi and Karamushka 2021). A safe supply of drinking water is still unavailable to 1.1 billion people, the majority of whom live in some of the world's poorest and emerging nations, according to reports from the United Nations (Hanif

et al. 2022). Access to safe drinking water is very important. However, the generation and improper disposal of the enormous quantities of harmful chemicals that multiple industries produce has only intensified the water crisis.

As such, numerous research articles and review papers on pharmaceutical compounds (PhCs) in water bodies have been published so far. Pharmaceutical compounds in wastewater (WW) and natural waters are typically low in concentration compared to other organic chemicals, and yet their human and veterinary use continues to grow. The highest PhCs concentrations are found in hospitals and nursing homes, where usage per person is significantly higher. The PhCs can also enter natural waters through waste from the pharmaceutical industry, aquaculture, and animal farming. Notably, among various PhCs, metformin hydrochloride (MFH) stands out as a leading anti-hypoglycemic drug, extensively used in diabetes treatment (Balakrishnan *et al*. 2022).

Metformin hydrochloride (MFH) was designated as a model essential medicine for hypoglycemia by the World Health Organization (WHO 2019). Often hailed as a wonder drug, MFH gained widespread use during the COVID-19 pandemic for treating patients, despite lacking firm evidence of its efficacy (Samuel *et al*. 2021). While its impact on treatment remains uncertain, it is recognized for helping maintain patient status. Following medical use, MFH can enter WW treatment systems. Unfortunately, traditional treatment plants struggle to effectively remove MFH from WW (Pap *et al*. 2023). Consequently, effluents from WW treatment plants that are added to receiving waters have been found to contain elevated concentrations of MFH. This has caused concern because MFH has been mentioned as a potential endocrine disruptor in the environment and is listed as a priority substance in the Chemical Investigations Programme (Li *et al*. 2021). Therefore, there is an urgent need to develop methods that can more sustainably, economically, and effectively remove antidiabetic PhCs from industrial effluents.

Methods such as photocatalysis (Kumar *et al.* 2021) ozonation (Scheurer *et al*. 2012), photolysis (Lin *et al*. 2020), and adsorption (Dave *et al*. 2024) have been investigated for eliminating MFH from WW. Adsorption's low costs, ease of use, superior performance, and environmental friendliness have all demonstrated its excellence and promise (Adeyi *et al*. 2023). Over the past few years, a wide range of materials, including carbon nanotubes, powdered activated carbon, chitosan, biochar, bottom ash, and organic resin, have been widely used to eliminate pollutants (Çavuşoğlu *et al*. 2021; Yang *et al*. 2024). Notably, these sorbents faced the issue of either low sorption capacities, high cost, or difficulties related to their reuse. Hence, there is a strong need to look for a low-cost, high-performance adsorbent material.

At present, fibrous adsorbents are widely used to purify water from pollutants as they are easily available, easy to use, reusable, and economical as well as possess highly active surface areas and mechanical strength to bring about chemical changes (Ma *et al*. 2020). As such, they are more adept at removing specific organic compounds from WW than conventional adsorbents, such as activated carbon.

Recently, the use of natural, inexpensive, non-toxic, and cellulose-based adsorbents for water and WW treatment has been extensively researched. Such adsorbents are typically sourced from agricultural biomass including sugarcane bagasse, rice straw, banana fibers, and cotton fibers. Cotton fibers, primarily composed of cellulose, have numerous hydroxyl groups that can be easily modified with various functional groups (*e.g.*, amino, cyclodextrin, carboxyl, as well as phosphorus or sulphur groups) to target specific pollutants (Bai *et al*. 2020).

Because of its many benefits such as its high efficacy, controllability, orderliness, and lack of need for catalytic or chemical reagents to illicit reactions, radiation-induced graft (RIG) polymerisation can be used to prepare fibrous adsorbents based on cotton fibers for use as bio-materials based adsorbents (M Saber *et al*. 2021). This process enables uniform treatment of the cotton fibers compared with untreated cotton. In addition, RIG provides higher grafting yield, shorter processing time, and improved penetration of the polymer within the fiber structure (Barsbay and Güven 2020). Currently, glycidyl methacrylate (GMA), a monomer with an epoxy group, is frequently utilized as a antecedent to create adsorbent that are polymeric for a range of uses that are centered on fibers, membranes, textiles, and films (Tahir *et al*. 2021). Furthermore, the modification of cotton fibers with phosphoric acid aims to incorporate phosphate functional groups onto the fiber surface, thereby enhancing surface acidity and creating negatively charged sites. These phosphate groups can effectively interact with the protonated amino groups of metformin through electrostatic attraction and hydrogen bonding. The presence of these groups is expected to raise the density of active adsorption sites and improve the binding affinity between the fibre surface and metformin molecules, resulting in improved adsorption efficiency.

It should be noted that MFH does not exist solely as a free cationic species in natural and wastewater systems. Due to its strong cationic character over a broad pH range, MFH readily forms stable ion pairs or charge-associated interactions with negatively charged natural constituents, including dissolved organic matter, humic and fulvic acids, inorganic anions, and bio-derived macromolecules. These interactions can partially shield MFH's positive charge, reducing its direct electrostatic attraction to negatively charged adsorption sites. Several studies have shown that such pre-existing complexes can significantly influence the mobility, bioavailability, and adsorption behavior of metformin in aquatic environments. Nevertheless, adsorption may still occur through mechanisms such as competitive displacement at high-affinity surface sites and hydrogen bonding, particularly for adsorbents with a high density of acidic functional groups (Zheng *et al.* 2024).

The present study developed an efficient adsorbent material from an economical fibrous material. In view of this, GMA was selected and utilised to graft natural cotton with emulsion-based RIG using electron beam (EB) to create cotton-*g*-GMA fibers. Phosphoric acid was later utilized to chemically functionalize the cotton-*g*-GMA for developing active sites on its surface.

The impacts of reaction time (RT) and solution quantity (SQ) were boosted to modify the grafted fibers. The developed adsorbent was characterized by various analytical tools such as thermogravimetric (TGA) analysis, Fourier transform infrared spectroscopy (FTIR), scanning electron microscopy (SEM), and X-ray diffraction (XRD). The adsorption of MFH from solutions that are aqueous in nature was carried out to investigate the performance of the phosphoric-cotton-*g*-GMA, which extant studies have failed to examine. Furthermore, many other variables of adsorption were also examined, like pH of MFH solution, adsorbent dose, temperature (*T*), initial MFH concentration (IMFHC), and contact time (CT). Moreover, the study revealed the adsorption mechanisms involved by deploying characterization, isotherms, kinetics, thermodynamics, and desorption (reusability) studies.

EXPERIMENTAL

Materials

The fibrous adsorbents were created using natural cotton fibers bought from local vendors (Malaysia). Glycidyl methacrylate (GMA, $C_7H_{10}O_3$) with 97% purity and Tween-20 (Tw-20; polysorbate 20) surfactant from Sigma-Aldrich (USA). The 85% phosphoric solution (phosphoric acid H_3PO_4) and industrial-grade propanol (C_3H_8O) were obtained from Merck (Germany). The chosen organic pollutant was metformin hydrochloride of formula $NH_2C(=NH)NHC(=NH)N(CH_3)_2$.HCl (Thermo Fisher Scientific, USA). All the received chemicals were utilized as such with no additional treatment.

Methods

Irradiation of natural cotton fiber substrate

To prevent the natural cotton fiber samples from coming into contact with oxygen (O_2), the samples were put in polyethylene Ziplock bags that has been de-aerated using nitrogen gas (N_2).

The sample-filled bags were then placed on solid carbon dioxide (dry ice) and moved through a conveyor to the irradiation chamber, where an NHV-Nissin® EPS3000 high-voltage EB accelerator (Japan) was used to irradiate the fibers. The accelerator operated under the following conditions: 1 to 20 m/min conveyor speed, 10 mA beam current, and 3 MeV acceleration energy. The samples received a radiation dosage of 10 kGy/pass.

Grafting Glycidyl Methacrylate on to the Irradiated Natural Cotton Fiber Substrate

The grafting mechanism proposed in (Ting *et al.* 2019) was used for performing the reaction of grafting. The samples that had been irradiated were placed in glass vials and then a vacuum pump was utilized for emptying the vials for 5 min. This grafting solution was produced by emulsifying the 5% GMA monomer and 0.5% Tw-20 solution-containing vials in 94.5% distilled water (DW) for 10 mins. They were purged of air and other gasses by bubbling them in purified N_2 for half an hour. Then, a tri-way stopcock was used to move the GMA monomers to the samples that had been irradiated. After they had been sealed, the vials were dipped in a 45 °C bath of water for 60 mins. The fibers were then removed, immersed, rinsed with propanol multiple times, and dried in a 50 °C oven.

The yield of the grafting was attained by means of gravimetry on the basis of this formula (Tahir *et al*. 2021):

$$GY\% = \frac{W_f - W_i}{W_i} \, x \, 100 \qquad (1)$$

Here, the starting weight of the sample before grafting is indicated by W_i while its weight after grafting is represented by W_f.

Functionalizing the Irradiated Cotton-*g*-GMA with Phosphoric Acid

The cotton-*g*-GMA was functionalized by treatment with phosphoric acid to integrate phosphoric groups onto the fibrous adsorbent's surface, thereby modifying the irradiated grafted fibers. For preparing the functionalization solution, a mixture of 10% phosphoric and 90% propanol was created in a double-necked, rounded-base flask and reflux heated at T=80 °C using a Daihan scientific Co. Ltd. WiseBath® digital water bath.

The grafted sample was then transferred to the solution and refluxed for a set duration at T=80 °C. The resulting phosphoric-cotton-*g*-GMA was thoroughly rinsed with methanol and dried in a 50 °C oven for a full day. The following formula was used to determine the incorporation of phosphoric groups (PhG) on the functionalized grafted fibers (Saber *et al*. 2023):

$$PhG = \frac{W_{Fg} - W_g}{W_{Fg}} \, x \, \frac{1000}{MW} \quad (2)$$

Here, phosphoric group is signified by PhG; W_{Fg} and W_{g}, respectively, represent the dry weights of the phosphoric-functionalized and samples that had been grafted; whereas MW represented the molecular weight of the phosphoric, which was 97.995 g/mol. Figure 1 depicts the radiation, functionalization, and grafting pathways.

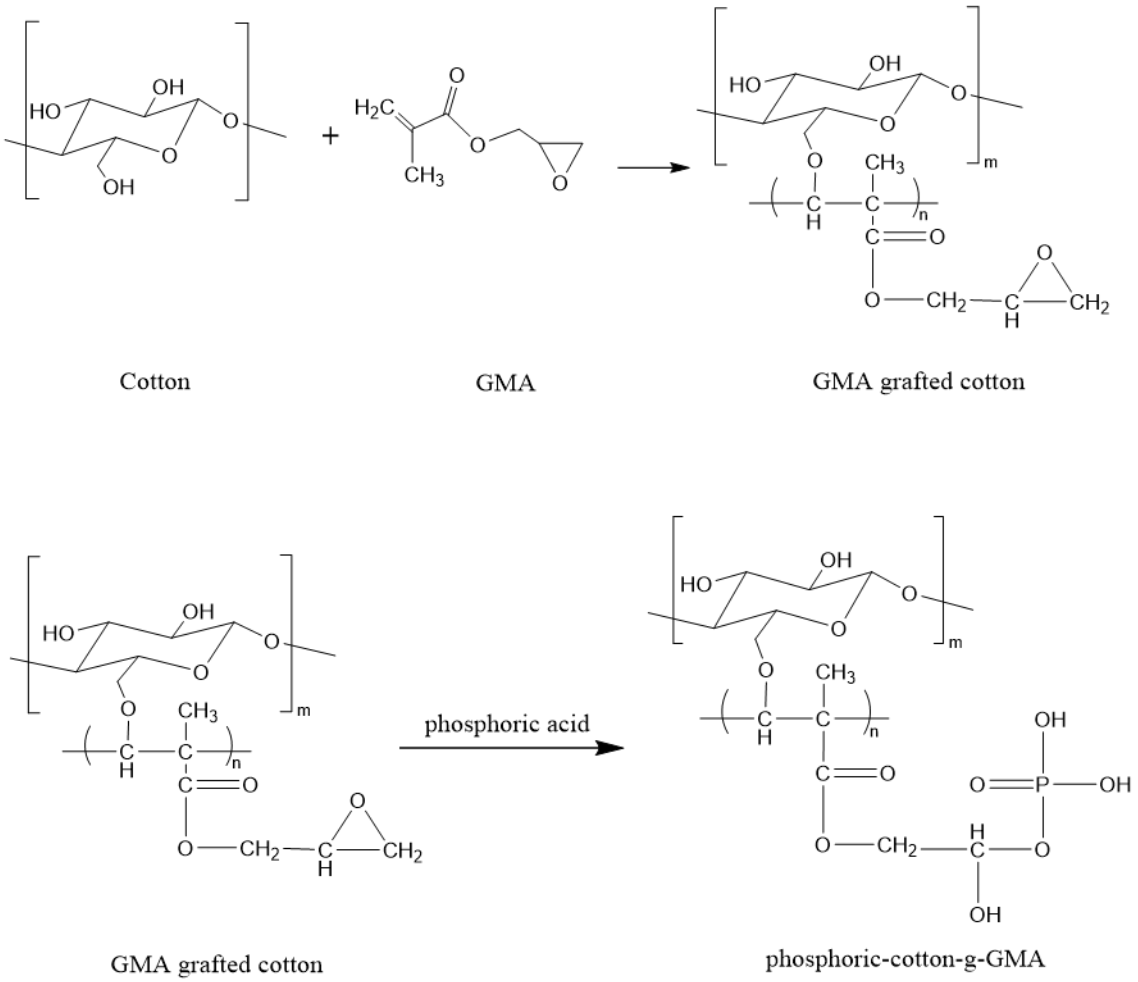

Fig. 1. An illustrational mechanism for the fibrous adsorbent preparation by GMA grafting onto natural cotton and subsequent functionalization with phosphoric acid.

Characterization of Adsorbent Material

The fibrous absorbent was characterized before and after functionalization using a Perkin Elmer® 1750X Fourier transform infrared spectrometer (FTIR, USA). The sample morphology was analyzed using a Hitachi® S-3400N SEM (Japan) with an acceleration voltage of 15 kV and a resolution of 500 µm. The samples' crystal structures were examined

using a Shimadzu® XRD-6000 (Japan). Moreover, the fibrous samples' thermal stability and degradation were measured by utilizing a Mettler Toledo® TGA/SDTA851 thermogravimetric analyzer (USA). The methodology suggested in (Jawad *et al*. 2020) was utilized to ascertain the phosphoric-cotton-*g*-GMA's pH at the point of zero charge (pH_{pzc}).

Examining the Metformin Hydrochloride Adsorption Capabilities of the Phosphoric-Cotton-*g*-GMA

Batch testing was conducted to determine the MFH adsorption capacity of the phosphoric-cotton-*g*-GMA. Distilled water (DW) was utilized to prepare a stock solution of 1.0 g/L MFH while aliquots of the solution were diluted to attain desired concentrations ranging between 5 and 50 mg/L before starting the experiments to observe the adsorption capacity. To prevent photo-oxidation, all measuring flasks comprising MFH were wrapped in aluminum foil. A set of 250 mL conical flasks was utilized in the experiments, placed in a temperature-controlled Sastec® ST-200R shaker-incubator with a shaking speed of 150 rpm and covered with a black cloth throughout the tests. The one-at-a-time (OVAT) methodology was used to attain the optimum findings. The impact of the amount of fibrous adsorbent contained on the adsorption of MFH was examined through varying the dosages of the phosphoric-cotton-*g*-GMA between 0.025 and 0.2 g. In addition, to evaluate pH's effects on absorption, the MFH solution's pH was attuned to range between 3 to 12 by utilizing 0.1 M hydrochloric acid (HCl) and 0.1 M sodium hydroxide (NaOH). The effect of *T* on adsorption performance was assessed by varying the *T* between 298 and 318 K. At specific intervals, aliquots of the solution were collected, strained, and the MFHC was computed by gauging its UV absorbance at 232 nm by utilizing a Shimadzu® UV-1800 spectrophotometer (Japan).

A total of five sorption and desorption cycles were carried out for analyzing fibrous adsorbent regeneration. A total of 15 mL of 0.1M NaOH was utilized to desorb the 0.05 g MFH that had been loaded onto the phosphoric-cotton-*g*-GMA. It was then washed and dried in a 50 °C oven for a full day before repeating.

Data Analysis Methods

The results reported were the average of the results of experiments that had been conducted thrice. The following formulas were used to determine the amount of MFH removed as well as adsorbed.

$$RE = \frac{C_o - C_e}{C_o}\ x\ 100 \quad (3)$$

$$q_e = \frac{(C_o - C_e)\,V}{m} \quad (4)$$

Here, C_o indicates the MFHC (mg/L) while C_e signifies the equilibrium concentration of the MFH (mg/L). The adsorbent mass (g) and volume of the $MFH_{(aq)}$ solution (L) were, respectively, indicated by m and V.

On the basis of the nonlinear models of pseudo-1st order (S. Langergren 1898), pseudo-2nd order (Ho and McKay 1999) and intraparticle diffusion (Weber and Morris 1963), kinetic studies in the context of adsorption were examined. The following nonlinear equations were utilized for defining the kinetic models.

Pseudo-1st order:

$$q_t = q_e\,(1 - e^{-K_1 t}) \quad (5)$$

Pseudo 2nd order:

$$q_t = \frac{q_e^2 K_2 t}{1 + q_e K_2 t} \quad (6)$$

Intra-particle diffusion:

$$q_t = K_{ip} t^{0.5} + C_{ip} \quad (7)$$

In these equations, the retention time (RT) is indicated by t (min), whereas K_1 (1/min) and K_2 (g/mg min), respectively, represented the constants for the adsorption rates of the pseudo-1st and -2nd order models. K_{IP} (mg/g min$^{0.5}$) represents the constant rate of the intra-particle diffusion for the intra-particle diffusion equation while q_e represents the amount of adsorbate adsorbed at equilibrium while q_t represented it at t.

Initial MFH concentrations (IMFHC) ranging from 5 to 50 mg/L were utilized to analyze the isotherms at equilibrium. The Langmuir (Armbruster and Austin 1938), Freundlich (Freundlich 1906), Temkin (Vinet and Zhedanov 2011), and Redlich-Peterson (Redlich and Peterson 1959) nonlinear isotherm models were employed, along with the equilibrium data, for ascertaining the constants of the model. The related nonlinear formulas were as follows.

Langmuir model:

$$q_e = \frac{q_{max} K_L C_e}{1 + K_L C_e} \quad (8)$$

Freundlich model:

$$q_e = K_F C_e^{\,1/n} \quad (9)$$

Temkin model:

$$q_e = \frac{RT}{b_T} \ln(k_T C_e) \quad (10)$$

Redlich Peterson model:

$$q_e = \frac{K_{RP} C_e}{1 + \alpha_{RP} C_e^{\beta}} \quad (11)$$

In these equations, q_{max} (mg/g) represents the maximum capacity for MFH adsorption, C_e (mg/L) represents the concentration of residual MFH adsorption at equilibrium, n indicates the inhomogeneity parameters related to surface of the adsorbent, and the universal gas constant is 8.314 J/mol and the absolute T was measured in Kelvin (K). The symbol α_{RP} indicates the affinity of the binding site and β indicates the exponent of the isotherm. Lastly, K_L (L/mg), K_F (mg/g)(L/mg)$^{1/n}$, K_T (L/mg), b_T (J/mol), and K_{RP} (L/g), respectively, represent the Langmuir, Freundlich, Temkin, and Redlich-Peterson parameters.

Furthermore, the adsorption's nature was determined using the R_L equilibrium parameter, which is a constant that is dimensionless, as seen in Eq. 12 (Saber *et al*. 2021).

$$R_L = \frac{1}{1 + K_L C_o} \quad (12)$$

Here, C_o and K_L, respectively, represent the initial MFHC (mg/L) and the adsorption constant of the Langmuir parameter (L/mg).

The fibrous adsorbent's regeneration capabilities were computed using the following equation:

$$Reg.\% = \frac{q_{e-reg.}}{q_{e-fresh}} \, x \, 100 \quad (13)$$

Here, the adsorption capacity of regenerated adsorbent is represented by $q_{e-reg.}$(mg/g) and the adsorbent capacity of fresh adsorbent is shown by $q_{e-fresh}$(mg/g) (Ferri *et al*. 2024).

Regression Analysis

The basis of the sum of square errors (*SSE*), coefficient of determination (R^2) and adjusted coefficient of determination (adj. R^2) were used to examine the inconsistencies between the theoretical and experiment-derived data of the models in Solver Add-ins, which is for Microsoft® Excel spreadsheets, and ascertain which model fit the data best. The formulas used to compute the *SSE* and R^2 are stated below.

$$R^2 = \frac{\sum(q_m - q_{cal})^2}{\sum(q_{cal} - q_m)^2 + \sum(q_{cal} - q_{exp})^2} \quad (14)$$

$$adj.R^2 = 1 - \frac{(1-R^2)(n-1)}{n-p-1} \quad (15)$$

$$SSE = \sum_{1}^{n}(q_{exp} - q_{cal})^2 \quad (16)$$

Here, for the experimental data, q_m (mg/g) represents the average adsorption capability, q_{exp} (mg/g) represents the adsorption capability, and q_{cal} represents the adsorption capability that had been determined (Wang and Guo 2020). Moreover, n and p represent the number of experimental data points and the number of model parameters, respectively.

RESULTS AND DISCUSSION

Radiation-Induced Grafting of Glycidyl Methacrylate on to Natural Cotton and Phoric-Functionalized Grafted Cotton

An EB was utilized to graft GMA onto natural cotton fibers, followed by treating the grafted cotton-*g*-GMA with phosphoric acid. The grafting reaction can initiate immediately on the natural cotton chains through the dual bonds in the GMA, as the radicals that were active were significantly reactive towards the GMA monomers. Samples were irradiated at an absorbed dose of 50 kGy for 60 min, whereby they achieved a grafting efficiency of 270% at reaction *T*=45 °C. The GMA's epoxy group acted as an antecedent that bound with other groups that were also reactive. The opening of the epoxy ring in the

GMA facilitates the formation of new groups that are functional. During the functionalization stage, covalent bonds are formed as phosphoric molecules attach to the grafted natural cotton fiber chains' epoxy groups. The density of the phosphoric functionalization was determined by calculating the density of the phoric (Eq. 2). The PhG was observed at different RTs and at different solution quantities (SQs).

The effect of RT on PhG quantity

The PhG intensified from 2 to 2.21 mmol/g when the RT was increased from one to two hours. This can be explained with regards to the fact that the PhG increase with RT. After which it decreased slightly as the RT increased (Fig. 2), indicating that the quantity of PhG did not significantly increase at longer RTs. The reason for this lackluster result could be that, after two hours, the epoxy sites on the GMA grafted cotton fibers are exhausted.

The effect of SQ on PhG quantity

The effect of 10:90 phosphoric-to-propanol ratios at SQs of 20, 30, and 40 mL on the PhG quantity were examined. The quantity of PhG increased as the SQ increased. For instance, the amount of PhG increased from 1.41 to 2.21 mmol/g when the SQ increased from 20 to 30 mL. This could be attributed to the better ability of the phosphoric to reach the epoxy sites of the cotton-*g*-GMA fibers. There might be a threshold, though, beyond which raising the phosphoric: propanol volume does not cause PhG to rise proportionately (Fig. 2). This is due to the possibility that the reaction will become saturated, in which case PhG will occupy all of the available binding sites on the fiber surface. Past this point, additional phosphoric quantity increases might not have a major effect on PhG. In fact, it could have an adverse effect due to the nature of the solution. Therefore, 30 mL was selected as the optimal SQ.

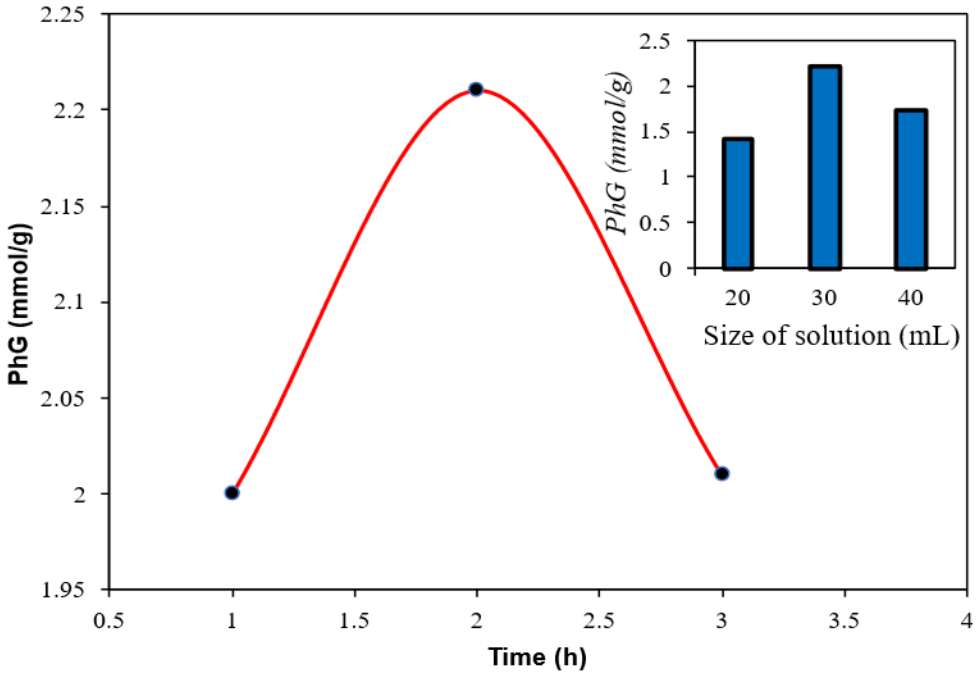

Fig. 2. The effect of time and medium size on functionalization reaction

Physiochemical Properties of the Materials-based Adsorbent

Morphology of the fibrous adsorbent

Scanning electron microscopy (SEM) was used to capture images and monitor changes on the surface of the fibers caused by GMA grafting and phosphoric functionalization. Figures 3a-d display SEM images of both untreated and treated cotton fiber samples. ImageJ was employed to assess fiber size distributions (Schneider *et al*. 2012). The untreated cotton fibers appeared flat and twisted. After treatment, SEM images revealed that the mean diameter of the cotton fibers increased from 16.15 to 24.44 µm following poly(GMA) grafting (Figs. 3a and 3b). Functionalization with phosphoric significantly expanded the fibers, resulting in an average diameter of 29.63 µm (Fig. 3c). This increase in size was attributed to the formation of a PhG layer around the grafted fibers. Additionally, the low absorbed dose during RIG ensured that the cotton fibers remained undamaged.

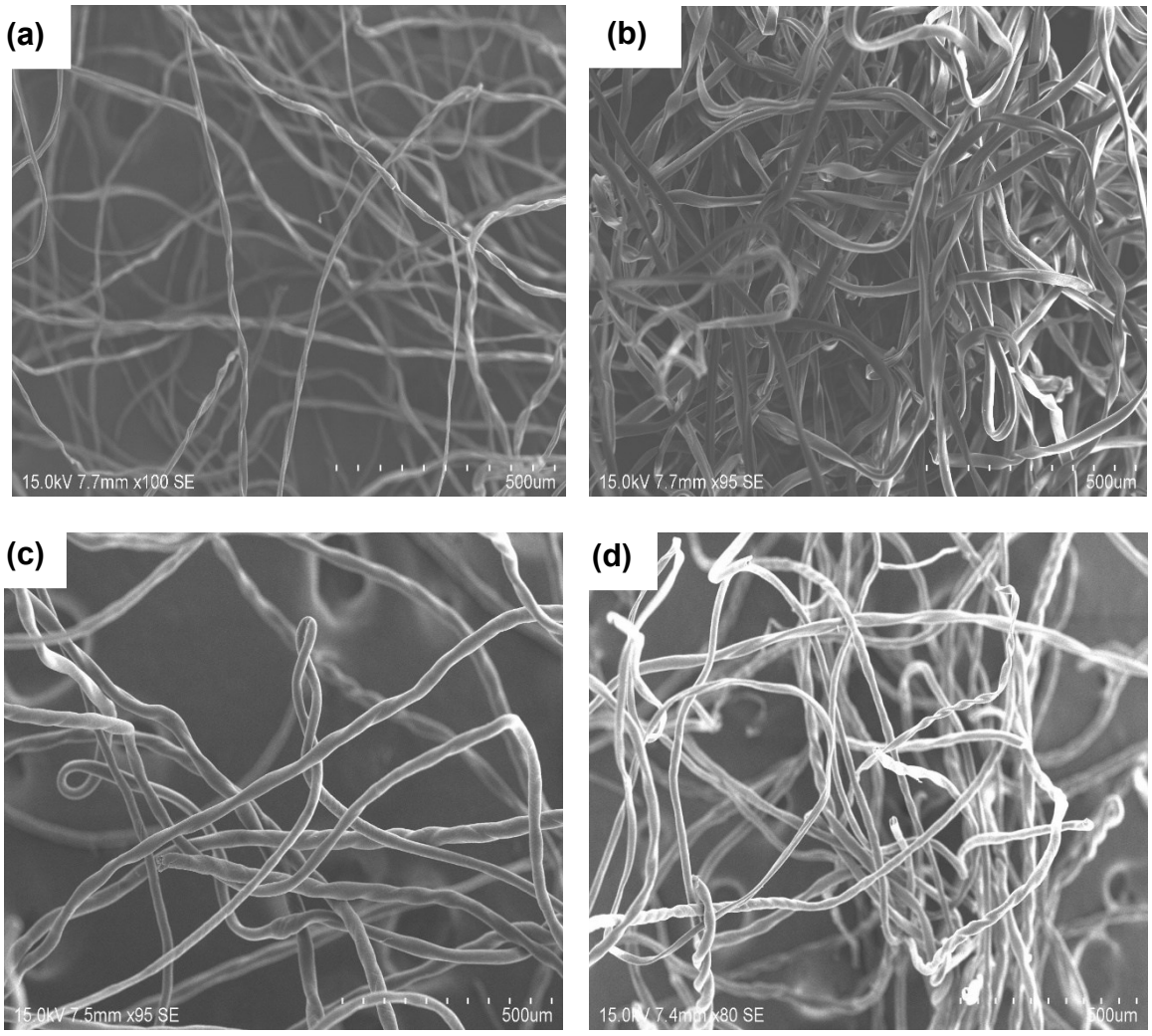

Fig. 3. SEM images of (a) natural cotton, (b) cotton-g-GMA, (c) phosphoric-cotton-g-GMA, and (d) MFH-phosphoric-cotton-g-GMA

Fourier Transform Infrared Spectroscopy Analysis

Figure 4 shows the FTIR spectra of the resulting phosphoric functionalized fibbers, GMA grafted cotton, and natural cotton. The mutual fibrous stretching at the stretching-

O-H absorbance at 3339 cm^{-1} represents the cellulose structure of cotton. The robust band at 1057 cm^{-1} is caused by the skeletal vibration of the pyranose C-O-C ring of the cellulose, while the spike at 1370 cm^{-1} indicates bending of the O-H in the cellulose glucose subunit's CH_2-OH group (Agathian *et al*. 2018).

After GMA grafting onto cotton fibers, absorbance bands appear at 1147 and 1728 cm^{-1}. These bands are caused by vibrational stretching of the C-O and C=O which are, respectively, derived from moieties of the GMA's -COO-ester bands at 996, 908, and 850 cm^{-1} produced by the epoxy ring (Korpayev *et al*. 2018). These results attest to successful GMA grafting onto the substrate made of cotton fibers.

Additionally, the functionalization with phosphoric acid resulted in a broad band at 3400 cm^{-1}, caused by the -OH groups' vibrational stretching due to the opening of the epoxy ring (Jeong *et al*. 2015; Mohamad *et al*. 2019). The bond at 1170 cm^{-1} was likely from the stretching P=O mode in the bonds of phosphate, while a small berm at this spike is from the vibrations of ionized $P^{+}-O^{-}$ found in the esters of the acid phosphate on the surface (Han *et al*. 2020). The GMA epoxy group peaks at 908 and 850 cm^{-1}, originally generated by stretching, nearly disappeared after functionalisation, therefore, the assimilation of phosphoric into the fibers that are GMA-grafted was complete (Abbasi *et al*. 2019; Galhoum *et al*. 2019). Moreover, the observed decrease in the epoxy-associated peaks at 908 and 850 cm^{-1}, along with the emergence of the phosphate-related band at 1170 cm^{-1}, provides supporting evidence of the epoxy ring-opening reaction and successful phosphoric acid functionalization.

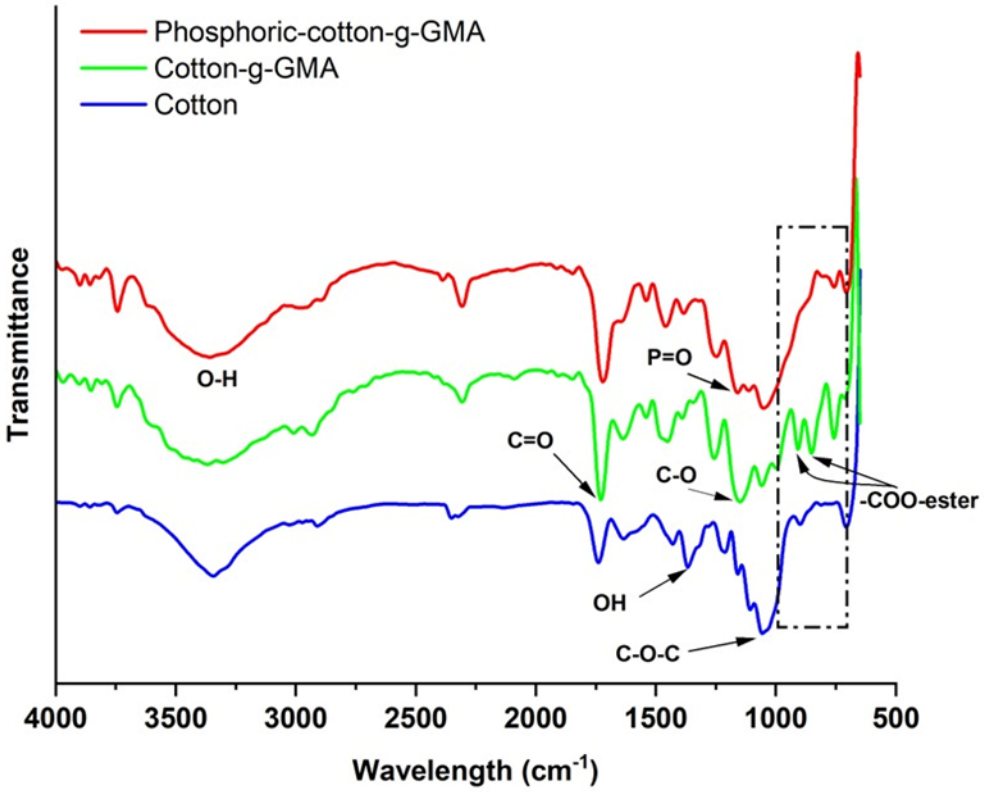

Fig. 4. FTIR spectra of natural cotton fibers, (cotton-*g*-GMA) (270% DG), and phosphoric-cotton-*g*-GMA

X-ray Diffraction Analysis

X-Ray diffraction (XRD) analysis was used to identify any alterations in the crystalline structure and determine how grafting and, later, functionalization impacted the cotton. Figure 5 displays the diffractograms for the natural cotton, GMA-grafted, and phosphoric-grafted cotton fibbers. The Scherrer formula, which is described below, was used to compare the crystallite size (L) to undertake intercalation:

$$L = \frac{k\,\lambda}{B\cos\theta} \quad (17)$$

Here, θ is the diffraction angle is by, k is a shape factor that had no dimensions but a standard 0.9, and B represents the breadth of the line when the intensity is half of the maximum intensity. Lastly, λ represents the wavelength of the Cu Kα radiation, which was 1.5406Å.

The crystalline parameters of natural cotton exhibited a peak at $2\theta = 22.63^{\circ}$ and L = 7.03 nm. After grafting, the addition of P(GMA) resulted in a peak at $2\theta = 22.67^{\circ}$ and a decrease in L to 8.43 nm for cotton-g-GMA, indicating a partial diminishment in crystallinity due to disruption of the ordered cellulose regions by the grafted polymer chains. After functionalization with phosphoric acid, there was a spike at $2\theta = 22.53^{\circ}$ and L = 10.29 nm, reflecting structural changes and the formation of phosphate groups. These observations confirm that the chemical modifications alter the crystalline structure while maintaining the overall integrity of the fibers.

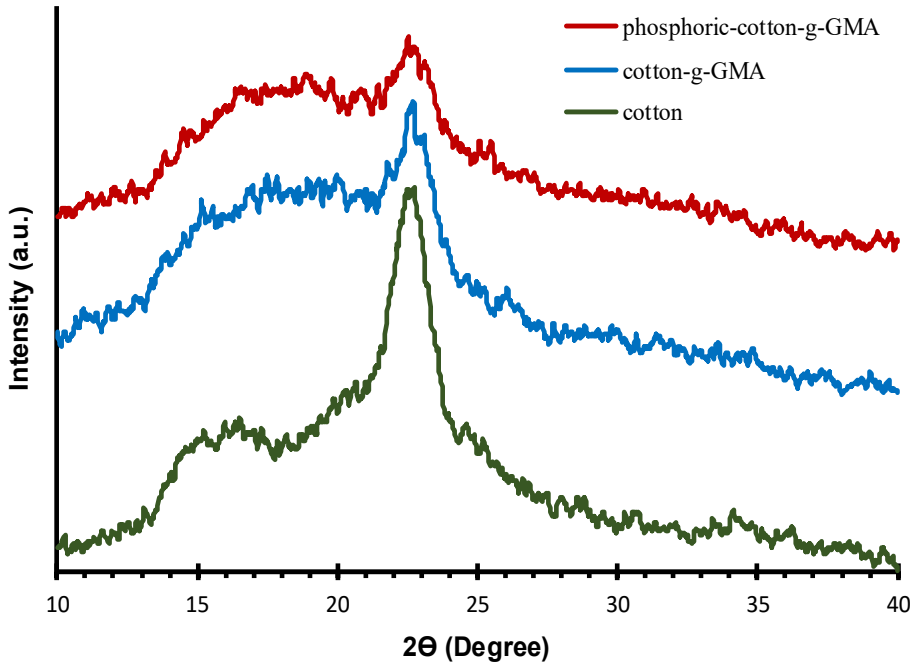

Fig. 5. XRD pattern of cotton, cotton-*g*-GMA and phosphoric-cotton-*g*-GMA

Thermal Stability of the Fibrous Adsorbent

Thermogravimetric and derivative thermogravimetric (TG-DTG) analysis was used to explain the thermal properties of virgin cotton fibers, as well as grafted and functionalized grafted cotton fibers. The study investigated the loss of mass, residue levels, and material degradation at a specific T. Figure 6 shows the thermogram of natural cotton,

revealing its decomposition behavior in a single step. In the initial phase, the natural cotton lost 5.7% of its mass before the *T* reached 120 °C, which is consistent with the evaporation of water molecules from the surface of its fibers. A minimal level of decomposition was observed in this stage due to a limited quantity of water molecules present. Additionally, the cotton undergoes thermal degradation (63.4%) between 242 and 541 °C in a two-step reduction process, with peaks in DTG at 345 and 483 °C.

As against natural cotton, the cotton-*g*-GMA fibers' thermal stability showed no mass loss up to 255 °C. Beyond this point, thermal degradation (67.13%) occurred between 274 and 386 °C, with the highest loss of weight occurring at around 309 °C. The increase in the amount of mass lost by the GMA-grafted sample was ascribed to epoxy groups and GMA ester degradation. Additionally, further thermal degradation (23.53%) of the cotton structure was observed between 391 and 553 °C (Bozkaya *et al*. 2021; Saber *et al*. 2023).

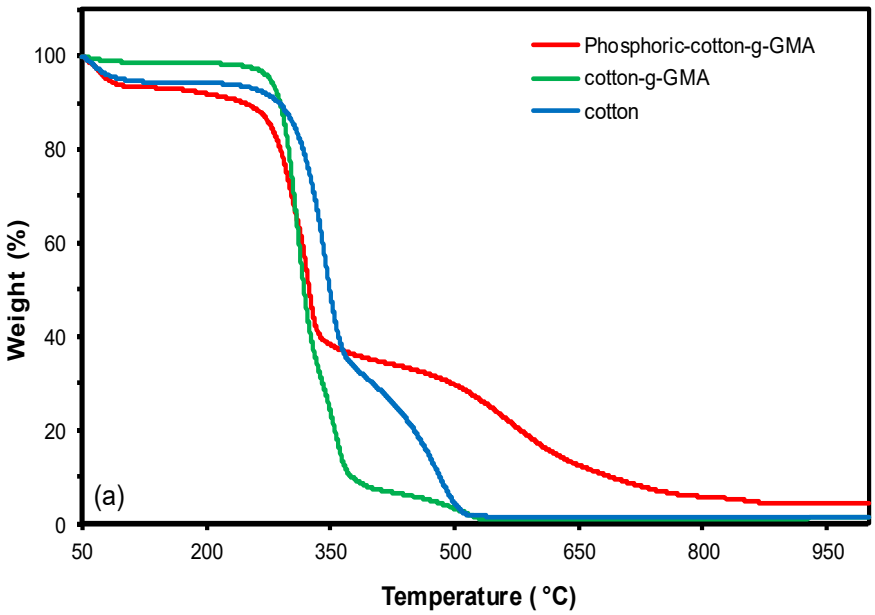

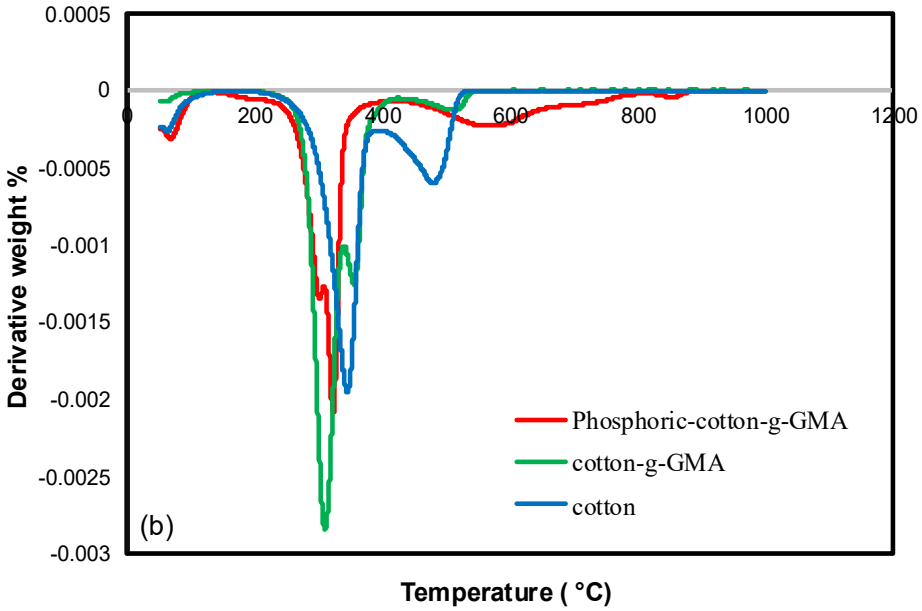

Fig. 6. TG-DTG curves of cotton, cotton-*g*-GMA (270% Dg), and phosphoric-cotton-*g*-GMA, (a) TG, (b) DTG

The phosphoric functionalization-grafted sample showed a stepwise decomposition behavior with distinct changeovers that accurately represented the contents of the cotton fibers. Mass loss variations were observed below 148 °C and at peaks of 68.8, 323, and 560 °C. These were related to water loss, PhG degradation, poly(GMA) graft degradation, and lastly, the degradation of the cotton substrate, in that order. At *T*=186 to 763 °C, the resulting weight loss ranged from 7.7% to 80.9%. Furthermore, phosphorus compounds are recognized for their ability to encourage the development of thermally stable char layers, which serve as a protective barrier that inhibits further thermal degradation. This investigation indicates that the phosphorylation of cotton fibers may not only boost their adsorption capabilities but also confer improved fire resistance, consistent with previous findings on phosphorus-containing cellulosic materials.

Factors Affecting MFH Adsorption Capabilities of the Phosphoric-Cotton-*g*-GMA

Adsorbent dose on MFH adsorption

The adsorbent dose was altered from 0.025 to 0.2 g to evaluate the MFH removal efficiency. As the adsorbent dose rose from 0.025 to 0.2 g, the MFH removal rose from 23.3% to 94.7%. This rise is credited to the expanded size of the contact area of the surface and the presence of an abundance of active sites on the fibrous adsorbent (Ding *et al*. 2021). Notably, when the adsorbent dose exceeded 0.1 g, MFH removal did not significantly improve. This was attributed to adsorption sites beginning to cluster or overlap, reducing the overall surface area accessible to MFH molecules (Hussain *et al*. 2021). In fact, the amount of MFH adsorbed decreased when the MFH adsorbent dose increased in the aqueous solution (Fig. 7). The reason behind this is that the adsorption capacity decreased as the adsorbent dosage level increased. Thus, after considering the influence of adsorption quantity and efficacy, along with economic costs, it was determined that 0.075 g of phosphoric-cotton-*g*-GMA was the most effective adsorbent dosage. A previous research

project showed similar findings on the effectiveness of using bio-char derived from *Phoenix reclinata* seeds to eliminate Cr(VI) ions (Katenta *et al*. 2020).

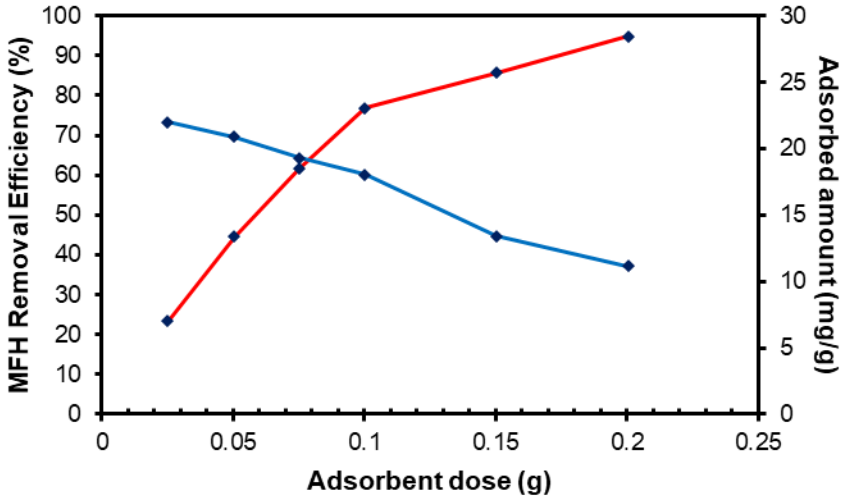

Fig. 7. Effect of adsorbent dosage to the MFH removal efficiency (IMFHC: 50 mg/L; time: 1 h; temperature 298 K and 150 rpm)

The impact of solution pH on MFH adsorption

The pH is a significant process variable that affects the degree of pollutant ionization and the surface attributes of the adsorbent, which has implications for the removal of pollutants using adsorbents (Aniagor *et al*. 2022). The pH level was adjusted between 3 and 12 to examine the effect on MFH adsorption onto phosphoric-cotton-*g*-GMA and better comprehend how it behaved. With adsorbent dose=0.075g, IMFHC=50 mg/L, CT=1.0 h, and shaking speed=150rpm, all other variables were held constant. As seen in Fig. 8(a), the MFH removal increased from 23.4% to 62.2% when pH was raised from 3.0 to 9.0. Maximum MFH removal was correlated with a pH of 10.0, after which pH levels gradually decreased. The explanation for the variation in MFH uptake with pH can be found in the pH_{pzc} of phosphoric-cotton-*g*-GMA.

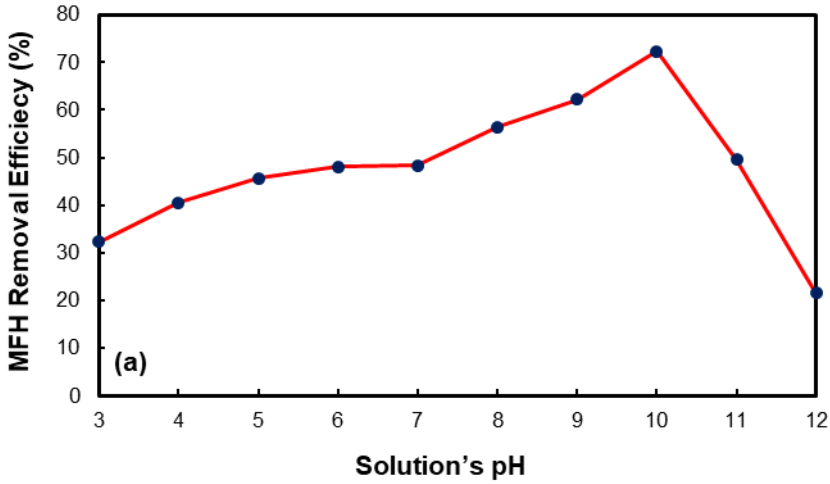

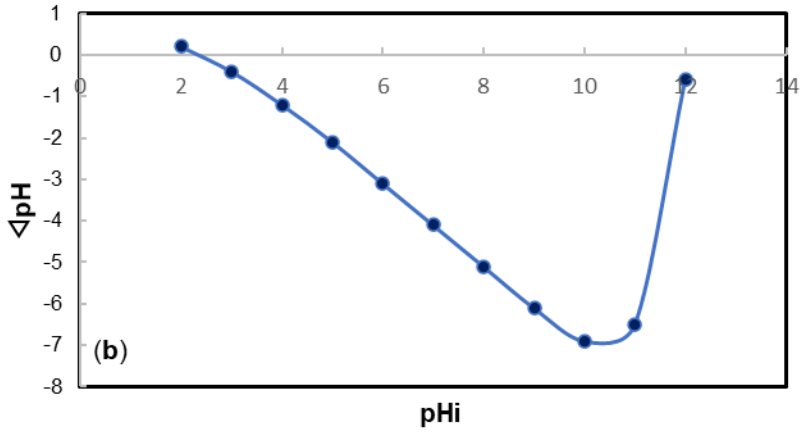

Fig. 8. (**a**) Effect of the solution's pH on MFH adsorption by phosphoric-cotton-*g*-GMA at different pH values (50 mg/L IMFHC, 0.075 g/50 mL adsorbent dosage, temperature 298 K, time 1 h and 150 rpm), (**b**) pH_{pzc} of phosphoric-cotton-*g*-GMA

As seen in Fig. 8(b), the phosphoric-cotton-*g*-GMA's pH_{pzc} was 2.5±0.1. At pH < pH_{pzc}, the adsorbent surface had more positively charged sites, resulting in low adsorption capacity. Conversely, at pH > pH_{pzc}, the surface of phosphoric-cotton-*g*-GMA became negatively charged due to deprotonation as the pH increased. This negative charge intensified the electrostatic attraction that occurred between the adsorbent surface and the MFH molecules, which are positively charged, enhancing MFH removal efficacy. These findings indicate that electrostatic forces and pH significantly affect MFH adsorption by impacting the contact among the molecules of the MFH and that of the adsorbent (Zhan *et al*. 2019). Moreover, the speciation of MFH also plays a crucial role in the adsorption behavior. The MFH exhibits a pKa value of approximately 12.4, corresponding to the protonation of its guanidine group. As a result, the MFH remained predominantly in its positively charged cationic form throughout the studied pH range (3 to 12). This consistent positive charge facilitated strong electrostatic interactions with the negatively charged surface of the phosphoric-cotton-g-GMA adsorbent at pH values higher than its pH_{pzc} (~2.5), further enhancing MFH adsorption. Thus, the observed pH effect can be attributed to the combined influence of adsorbent surface charge and MFH speciation behavior. As the optimal MFH removal occurred at pH=10, all subsequent adsorption experiments were conducted under this condition.

Temperature Impact on MFH Adsorption

Temperature (*T*) was also looked into because it plays a major role in both the physisorption and chemisorption processes. Regardless of whether the *T* is favorable or not, the impact of *T* is determined by the chemical and physical properties of the adsorbate and adsorbent and the kind of reaction between them. The rate of endothermic chemical reactions typically rises with *T*, whereas the relationship between *T* and exothermic reactions is the inverse (Aniagor *et al*. 2022).

This study utilized three *T*s (298, 308, and 318 K) to evaluate the influence of *T*. The experimental work was carried out using adsorbent dose=0.075 g and pH=10. The research concluded that the adsorption of MFH increased as the *T* was increased, reaching a high removal percentage of 76.9% on phosphoric-cotton-*g*-GMA at 308 K. This could be attributed to the higher kinetic energy of the MFH at 308 K, which raises the likelihood of contact among the MFH and sites that are active on the surface of the fibers (Aniagor *et al*.

2022). However, MFH reduction decreased at 318 K (Fig. 9). A higher *T*, above 308 K, enhanced the diffusion of mass and solubility of MFH in water, while weakening the bonding forces between adsorbent sites and adsorbate, leading to increased desorption of MFH into the fluid phase (Arnata *et al*. 2019).

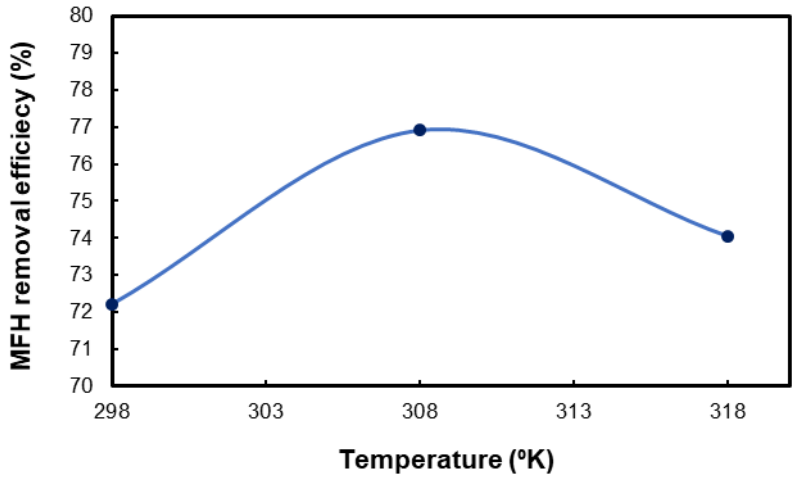

Fig. 9. Effect of temperature on MFH removal efficiency by phosphoric-cotton-*g*-GMA (adsorbent dose: 0.075 g/50 mL; IMFHC: 50 mg/L, pH 10, time: 1 h and 150 rpm)

The impact of initial metformin hydrochloride concentration on adsorption rate over time

Six initial metformin hydrochloride concentrations (IMFHC) ranging from 5 to 50 mg/L were tested to evaluate adsorption efficacy relative to contact time (CT), assessing the impact of CT and IMFHC on adsorption equilibrium. The experimental conditions remained constant: Adsorbent dose=0.075 g, pH=10, and *T*=308 K. The change in IMFHC over CT was monitored, and Eq. 4 was used to calculate the amount of MFH that was adsorbed by the phoric-cotton-*g*-GMA (q_e). Results showed that MFH was rapidly adsorbed onto the phoric-cotton-*g*-GMA surface, with overall adsorption increasing with CT until reaching equilibrium (Fig. 10). The swift and effective adsorption was attributed to the numerous active functional groups on phosphoric-cotton-*g*-GMA. Additionally, MFH adsorption proportionally increased with higher IMFHC (Fig. 10). This was due to the higher concentration gradient driving MFH molecules towards sites of adsorption that are active, thereby overpowering the resistance of the transfer of mass from the phase of water to the surface of the adsorbent (Akhtar *et al*. 2016; Aarab *et al.* 2020).

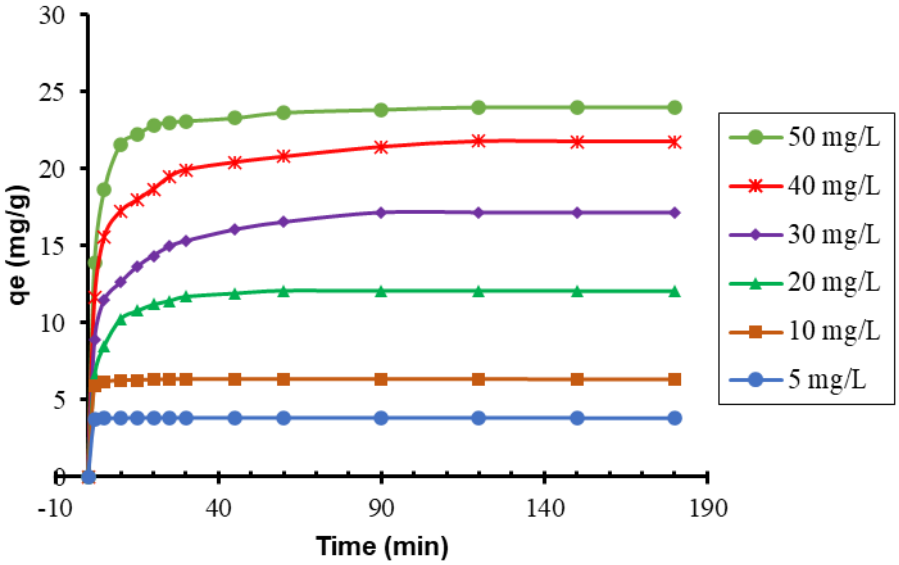

Fig. 10. Effect of CT and IMFHC on the adsorption of MFH by phosphoric-cotton-*g*-GMA (adsorbent dose = 0.075 g, pH 10, temperature = 308 K, agitation speed = 150 r/min, and volume of solution = 50 mL)

Metformin Hydrochloride Adsorption Process onto Phosphoric-Cotton-*g*-GMA

Kinetics of adsorption

The results of kinetic experiments were used to determine the nature of the reaction involved in MFH adsorption, as well as the speed of MFH elimination and the way in which MFH spread onto phosphoric-cotton-*g*-GMA. The pseudo-1st order (Eq. 5), pseudo-2nd order (Eq. 6), and intraparticle diffusion (Eq. 7) equations were deployed to fit the kinetic data of the adsorption (Figs. 11a-c and Table 1). The models provided a good fit for the fibrous adsorbent samples' kinetic data, as indicated by the high R^2 and low *SSE* values. The pseudo-2nd order kinetic model resulted in a maximal R^2 (> 0.99) and minimal *SSE*, while also providing adsorption amount (q_{cal}) similar to experimental values (q_{exp}). It was concluded that the adsorption rate is governed by diffusion processes within the fibrous matrix rather than by simple surface reaction kinetics.

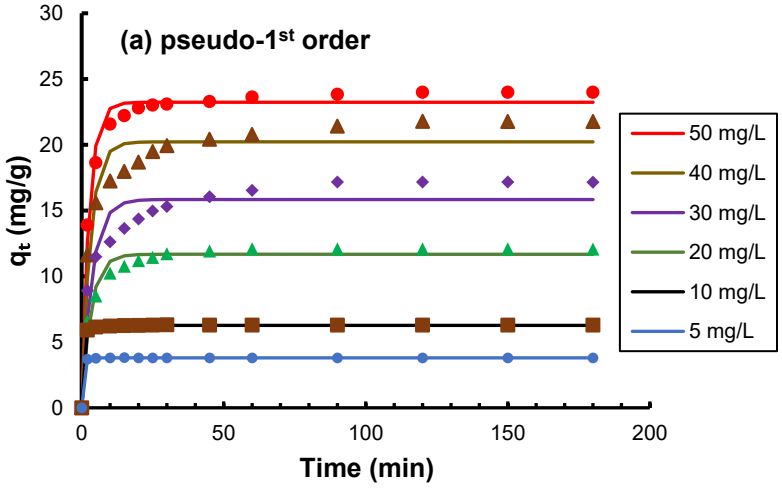

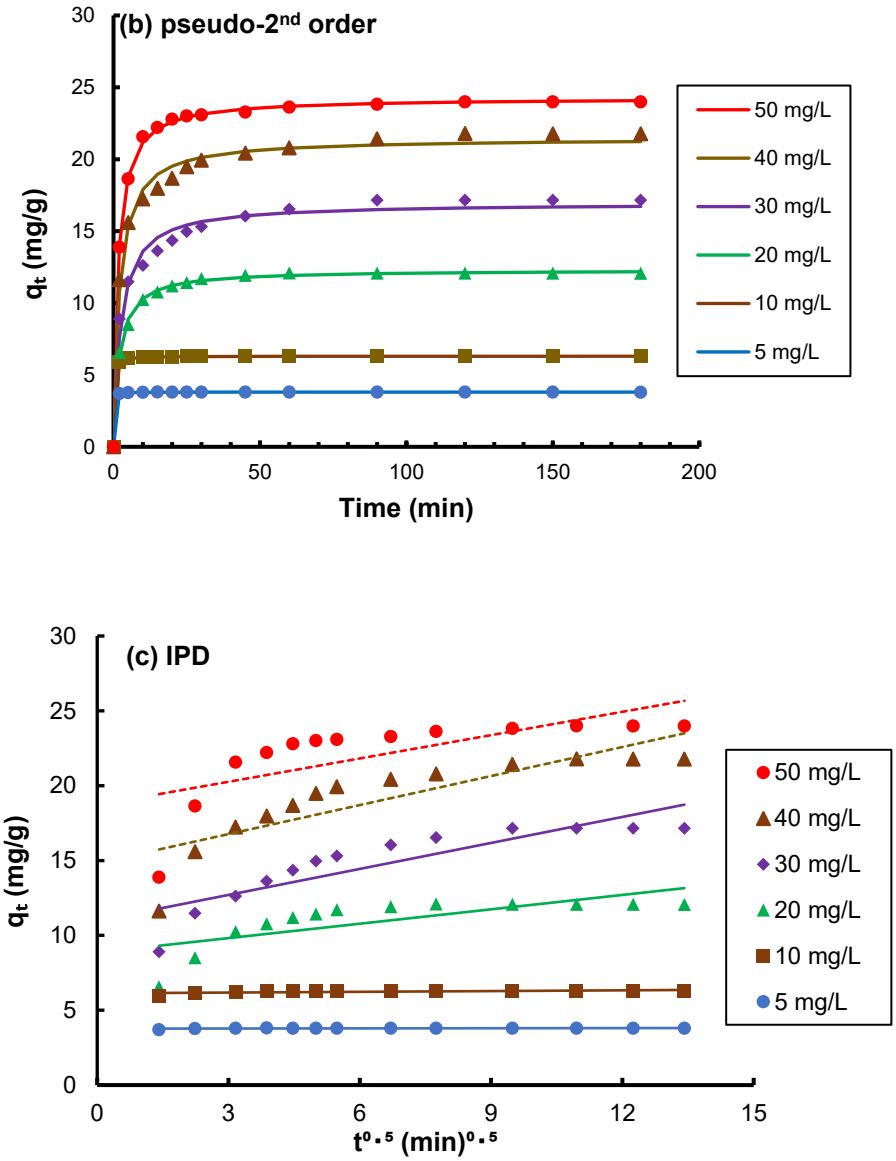

Fig. 11. Use of various models to fit the kinetic data recorded for the adsorption of MFH onto phosphoric-cotton-*g*-GMA (q_t: amount of MFH adsorbed at time t (min) *via* the nonlinear regression method; (a) pseudo 1st order, (b) pseudo 2nd order and (c) intra-particle diffusion linear model, the MFHC was varied (5 - 50) mg/L

Both PFO and PSO models are empirical in nature and ought not be directly interpreted in terms of specific chemical mechanisms (Hubbe *et al.* 2019). The good fit of the PSO model in this work is consistent with diffusion-controlled adsorption occurring within the structure of micro- and mesopores in the modified fibers (Aarab *et al.* 2020; Huang *et al.* 2016). Previous research showed that the pseudo-2nd order model is better suited for describing the kinetics of MFH adsorption on various adsorbents such as an iron-biochar composite (Pap *et al*. 2023).

It was crucial to determine how adsorption took place. The intraparticle diffusion model was utilized for further examination of the limited step in the MFH's rate of diffusion onto the phosphoric-cotton-*g*-GMA. The four main stages of the process of adsorption were identified. The initial stage included the transfer of the adsorbate, from the

bulk of the solution to the layer that was adjacent to the adsorbent. The molecules that diffused through the layer in the second and third stages until they reached the adsorbent and travelled throughout the pores on the surface of the adsorbent. The fourth step included the adsorbate being adsorbed by the adsorbent.

Table 1. The Parameters of Kinetics Models for MFH Adsorption on Phosphoric-Cotton-*g*-GMA

Parameter (s)	MFH Initial Concentration (mg/L)					
	5	10	20	30	40	50
q_{exp} (mg/g)	3.814	6.307	12.097	17.160	21.787	23.994
Pseudo-1st order						
q_{cal} (mg/g)	3.798	6.269	11.675	15.837	20.225	23.233
K_1 (1/min.)	1.828	1.43	0.31	0.278	0.334	0.39
R^2	0.999	0.999	0.972	0.922	0.946	0.998
SSE	0.001	0.024	4.454	24.158	25.377	8.174
Pseudo-2nd Order						
q_{cal} (mg/g)	3.807	6.306	12.305	16.948	21.463	24.269
K_2 (g/mg min.)	4.889	1.193	0.042	0.024	0.024	0.028
R^2	0.999	0.999	0.998	0.981	0.968	0.999
SSE	0.001	0.002	0.337	5.654	4.390	0.311
Intraparticle Diffusion Model*						
C_{ip} (mg/g)	2.854	4.642	48.086	74.315	82.026	82.026
K_{ip} (mg/g $min^{0.5}$)	0.108	0.188	3.158	4.567	5.428	5.428
R^2	0.194	0.214	0.503	0.503	0.504	0.518
* Represented the calculated parameters derived from the linear model.						

At least one of these stages was found to be the controlling factor in the adsorption process, known as the rate-limiting step. In recognizing this stage, the beginning and ending stages can be disregarded, as they are typically rapid (Weber and Smith 1987; Magdy *et al.* 2018). The intraparticle diffusion model was used by plotting q_t against $t^{0.5}$ to identify the controlling step. If the line dissected the original line, intraparticle diffusion was the only mechanism accountable for adsorption. If not, the rate-limiting step involves additional phases such as intraparticle diffusion, pore diffusion, and surface chemical reactions (Huang *et al*. 2016; Jiang *et al*. 2019; Masinga *et al*. 2022).

As illustrated in Fig. 11c, the plots of the Weber and Morris models that had been linearized (regression lines) did not dissect the original lines. Because $R^2 < 0.9$, it can be concluded that intraparticle diffusion was not the sole rate-limiting step in the adsorption of MFH by phosphoric-cotton-*g*-GMA. Therefore, adsorption likely relied on manifold procedures, including adsorption *via* the surface and diffusion between particles. Similar

findings were reported in previous studies using modified nano-biochar from artichoke leaves for the MFH anti-diabetic drug's adsorption (Mahmoud *et al*. 2020).

Adsorption isotherms

Adsorption isotherms were utilized to explain the phenomena occurring during the MFH adsorption process, in particular how the adsorbate interacted with the adsorbent, and to show the association between the adsorption capacity of phosphoric-cotton-*g*-GMA and the MFH concentration in the solutions left over when the adsorption was at equilibrium. In order to achieve this, the nonlinear models of Langmuir (Eq. 8), Freundlich (Eq. 9), Temkin (Eq. 10), and Redlich-Peterson (Eq. 11) were used. The Langmuir model is centered on the idea that adsorption occurs in a single layer on a homogeneous adsorbent surface. By computing the separation factor R_L, additional evaluation was conducted to determine the suitability of monolayer adsorption and surface homogeneity. At $0 < R_L < 1$, it is considered positive adsorption; $R_L > 1$ indicates negative adsorption; $R_L = 1$ signifies adsorption that is linear, while $R_L = 0$ indicates that the adsorption cannot be reversed (Abin-Bazaine *et al*. 2022).

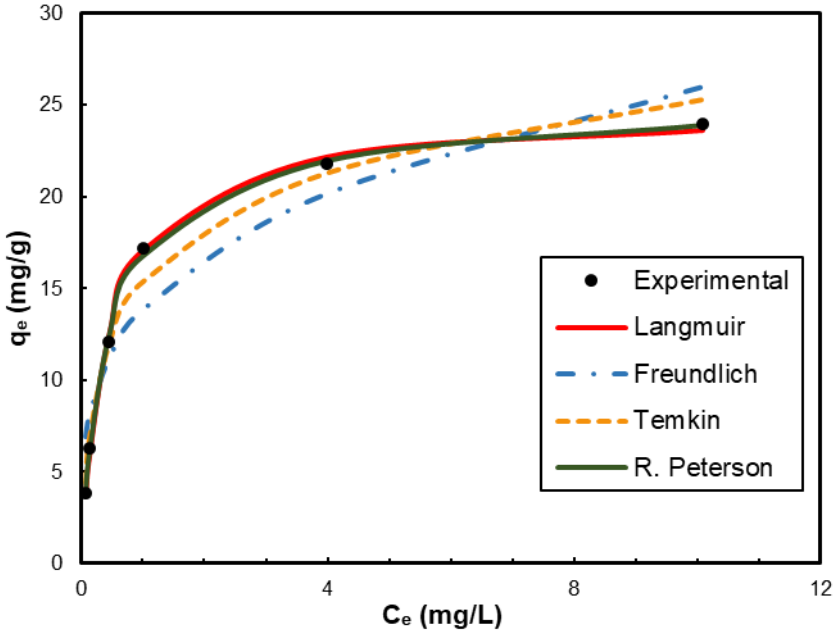

Fig. 12. Isotherm models used to fit experimental data for the MFH adsorption on phosphoric-cotton-*g*-GMA fibrous *via* Langmuir, Freundlich, Temkin, and Redlich Peterson at 308 K, pH 10, adsorbent dose = 0.075 g, volume of solution = 50 mL and agitation speed = 150 rpm

Table 2. The Parameters of Isotherm Models and Equilibrium Parameters for MFH Adsorption on Phosphoric-Cotton-*g*-GMA

Isotherm Model (s)	Parameters		R^2	adj. R^2
Langmuir	q_{max} (mg/g)	24.679	**0.998**	**0.997**
	K_L (L/mg)	2.214		
	SSE	0.638		
Freundlich	K_F (mg/g)(L/mg)$^{1/n}$	13.825	**0.898**	**0.831**

	N	3.657		
	SSE	30.97		
Temkin	K_T (L/mg)	34.461	**0.983**	**0.972**
	b_T (J/mol)	591.858		
	SSE	5.68		
Redlich-Peterson	K_{RP} (L/g)	60.065	**0.998**	**0.997**
	α (L/mg)	2.591		
	B	0.968		
	SSE	0.338		
Separation Factor (R_L)	**C_o (mg/L)**	**R_L**		
	5	0.0829		
	10	0.1355		
	20	0.0036		
	30	0.009		
	40	0.0008		
	50	0.0006		

The Freundlich model is empirical and depicts adsorption by the multiple layers of an adsorbent that has a surface that is heterogeneous. Moreover, 1/n illustrates the intensity of the adsorption that occurred. The adsorption is considered positive if $0 < 1/n < 1$, negative if $1/n > 1$, and cannot be reversed if $1/n=1$ (Musah *et al*. 2022).

The Temkin isotherm explains the relationship between the adsorbent and adsorbate through equal binding energy distribution, resulting in a linear decrease in heat of adsorption as adsorbate coverage rises. K_T is the constant of Temkin, reflecting the energy for binding, while b_T signifies the adsorption's heat. The b_T indicates if the adsorption is either endothermic or exothermic. If $b_T > 0$, heat was discharged and it's exothermic. If $b_T < 0$, heat was absorbed and it's endothermic (Batool *et al*. 2018; Saxena *et al*. 2020).

The Redlich–Peterson model is an empirical three-parameter model that blends the features of both the Freundlich and Langmuir models (Majd *et al*. 2022). The exponent *β* typically ranges from 0 to 1. When β is close to one, the model aligns more with Langmuir adsorption, while a β value close to zero indicates that Freundlich is the dominant isotherm (Kalam *et al*. 2021).

Figure 12 shows how the isotherm model fits the data for the MFH adsorption that was equilibrium on phosphoric-cotton-*g*-GMA, with the corresponding parameters of the isotherm provided in Table 2. All the isotherm models presented excellent agreement with the data of the experiment as their R^2 values were in the range 0.898 to 0.998. With the highest R^2 (0.998) and lowest *SSE* (0.338), the Redlich-Peterson model fit the data best, therefore, the Freundlich and Langmuir isotherms played a role in the adsorption. The parameter β in the Redlich-Peterson isotherm model was based on the Langmuir equation, which yielded a high R^2 of 0.998, which is close to 1. The Langmuir isotherm showed a

positive shape in describing the chemical adsorption as R_L = 0.0006 to 0.1355. Moreover, the Freundlich model also exhibited a positive shape as l/n means that the intensity of the adsorption was 0 to 1.

Thermodynamic Functions

Temperatures (T) ranging from 298 to 318 K were utilized in the thermodynamic analysis of the adsorption of MFH by phosphoric-cotton-*g*-GMA fibers. The formulas below were used for ascertaining the thermodynamic parameters of Gibb's free energy change (ΔG^{o}), enthalpy change (ΔH^{o}), and entropy change (ΔS^{o}):

$$\Delta G° = -RT \ln k_d \quad (18)$$

$$\ln k_d = \ln \left[\frac{q_e}{C_e}\right] = \frac{\Delta S°}{R} - \frac{\Delta H°}{RT} \quad (19)$$

Here, the T was measured in K, R represented the perfect gas constant (8.314J/mol K), and k_d represented the distribution coefficient for linear sorption (q_e/C_e). The $1/T$ was plotted against the ln k_d according to the Van't Hoff equation (Fig. 13).

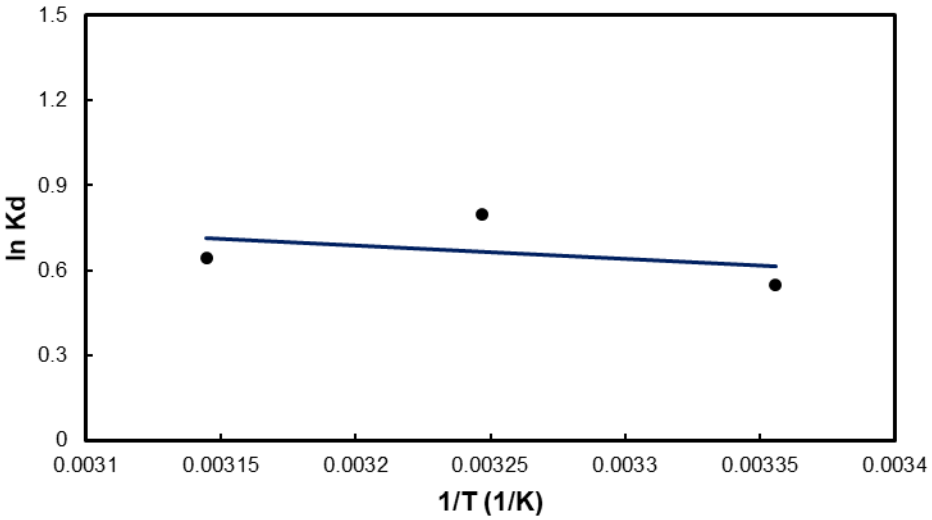

Fig. 13. Van't Hoff plot for MFH adsorption onto phosphoric-cotton-*g*-GMA (adsorbent dose = 0.075 g, volume of solution = 50 mL, pH 10 and agitation speed = 150 rpm)

Table 3 presents the calculated thermodynamic parameters. The feasibility of the procedure was confirmed, with MFH adsorption onto phosphoric-cotton-g-GMA being spontaneous due to a negative ΔG^{O}. The small positive value of ΔH^{O} indicates the fact that adsorption had a weak temperature dependence rather than being distinctly endothermic. Raising the temperature from 298 to 308 K resulted in a higher removal of MFH (Fig. 13) and increased the adsorptive capacity, which is reasonable considering the adsorption and diffusion processes involved. Moreover, there was a rise in "randomness" at the interface of the solid-solution in the adsorption as the ΔS^{O} was positive.

Table 3. Thermodynamic Parameters for MFH Adsorption on Phosphoric-Cotton-*g*-GMA

T (K)	k_d	ΔG° (kJ/mol)	ΔH° (kJ/mol)	ΔS° (kJ/mol. K)
298	1.733	-1.362		
308	2.222	-2.045	3.838	0.018
318	1.902	-1.699		

Regeneration Potential of Phosphoric-Cotton-*g*-GMA

When evaluating adsorbent efficacy in treating WW, it is crucial to take reusability into account. To evaluate their recyclability and performance over multiple cycles, the phosphoric-cotton-*g*-GMA was impregnated with MFH then washed and reused multiple times. To that end, 0.1M HCl was used, with the recycling process repeated five times (Fig. 14). The recovery of MFH was nearly 94.65% in the final cycle. This indicates that phosphoric-cotton-*g*-GMA fibers are stable and can be regenerated for reuse with proper performance. Thus, the process is sustainable and implementable in a cheap and eco-friendly manner.

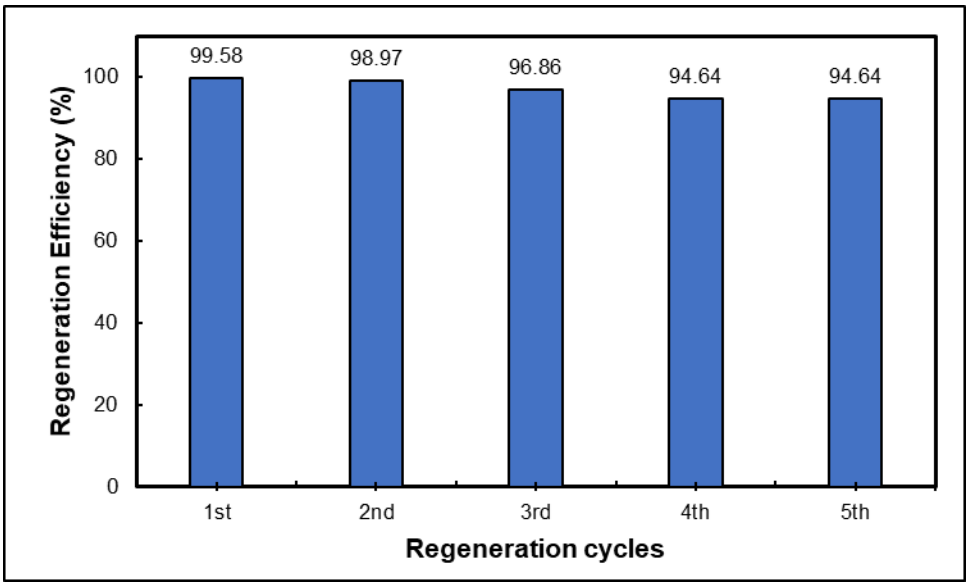

Fig. 14. Regeneration of phosphoric-cotton-*g*-GMA after MFH loading

Proposed Adsorption Mechanism

Based on the results of the experiments and theoretical analysis of the multiple interactions that occurred between the MFH and fibrous adsorbent, the manner of the adsorption of MFH on phosphoric-cotton-*g*-GMA was determined (Fig. 15). Numerous variables affect adsorption, such as the surface of the adsorbent, the MFH's structure on a molecular level, and how it interacted with the adsorbate. The adsorption of MFH is greatly influenced by the pH of MFH, with higher pH levels being more favorable for adsorption, leading to a greater amount of MFH being adsorbed. This was attributed to the robust intermolecular electrostatic attraction among the negatively charged adsorbent of phosphoric-cotton-*g*-GMA surface and the positively charged MFH. Hydrogen bonding is another potentially important contribution to the binding interactions between the MFH molecules and phosphoric-cotton-*g*-GMA, where the N_2 of MFH can basically bind with the -OH groups on the surface of functionalized fibers (Khan *et al*. 2021). Therefore, electrostatic interactions, H-bonding, and complexation phenomena synergistically and significantly enhance the adsorption efficiency of the fibers. Moreover, π–π stacking may further stabilize the adsorbed layer, but these effects may be minor relative to the dominant electrostatic interactions. These outcomes substantiated the effective adsorption of MFH on the fibrous adsorbent.

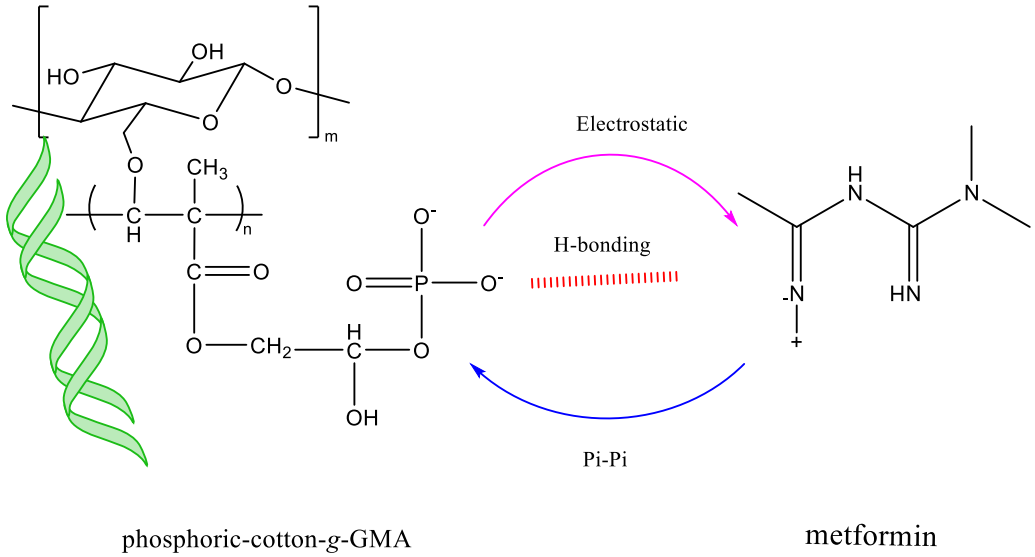

Fig. 15. Elucidation of the proposed mechanism for MFH adsorption onto phosphoric-cotton-*g*-GMA

Adsorption Efficacy of Phosphoric-Cotton-*g*-GMA *vs.* Other Adsorbents

As seen in Table 4, the phosphoric-cotton-*g*-GMA was found to be a better adsorbent than the materials discussed in other studies. Its adsorption capabilities were not only significantly higher (24.7 mg/g), but it was also faster and more accurate and environmentally-friendly than comparable methods. It can also be reused as many as five times with high performance, which is not the case for many of its counterparts (Table 4). The outstanding MFH adsorption capabilities of the phosphoric-cotton-*g*-GMA could be attributed to the efficient grafting of GMA on to irradiated natural cotton followed by the functionalization of its surface with phosphoric group.

Table 4. Comparison of the Adsorption Capacity of MFH *via* Various Adsorbents

Adsorbent	*Q* mg/g	References
Silica-Alumina Composite	46	(Alnajjar *et al*. 2019)
Fe-ZSM-5 (Fe-Z) Zeolite	14.99	(Niaei and Rostamizadeh 2020)
MOM-Fe_3O_4	9.67	(Cusioli *et al*. 2020)
M-MWCNT	26.17	(Çavuşoğlu *et al*. 2021)
Hydrochar Activated from Byrsonima	113.6	(Sanchez-Silva *et al*. 2022)
Phosphoric-Cotton-*g*-GMA	**24.7**	**This Study**

CONCLUSIONS

1. An electron beam (EB) methodology was adopted for glycidyl methacrylate (GMA)-grafting on cotton through radiation-induced graft (RIG) polymerisation. The GMA emulsion grafting on cotton fiber was achieved at 45 °C with an absorbed dose of 50 kGy for 60 min, resulting in a grafting percentage of 270%. The grafted fibers were then functionalized with phosphoric acid. The impacts of retention time (RT) and solution quantity (SQ) during functionalization were examined.
2. Successful introduction of graft polymerisation was confirmed by scanning electron micrograph (SEM) images and Fourier transform infrared (FTIR) analysis of GMA's -COO-ester bands at 996, 908, and 850 cm^{-1} produced by the epoxy ring. The bond at 1170 cm^{-1} were from the stretching P=O mode in the bonds of phosphate, which confirmed successful incorporation of phosphoric group into prepared grafted fibers.
3. The phosphoric-cotton-*g*-GMA was tested for its capability to eliminate metformin hydrochloride (MFH) from aqueous solutions. The optimal adsorption parameters were absorbent dose=0.075 g, pH=10, *T*=308 K, and CT=2 h. Kinetic analyses indicated that MFH adsorption followed a pseudo-2nd order model. The Redlich-Peterson isotherm model best fit the data for phosphoric-cotton-*g*-GMA, with the β exponent near one and a high R^2 (0.998) based on the Langmuir isotherm model. The maximal capacity for MFH adsorption of the phosphoric-cotton-*g*-GMA was 24.7 mg/g. Furthermore, the MFH adsorption procedure was spontaneous and endothermic.
4. The phosphoric-cotton-*g*-GMA could be regenerated using a small concentration of HCl, maintaining high performance for at least five recycling recurrences. Thus, the phosphoric-cotton-*g*-GMA can successfully be used to adsorb MFH from aqueous solutions.
5. Future studies should focus on optimizing the regeneration process to minimize the formation of secondary effluents and improve the recovery of MFH. This could include investigating alternative desorption agents, developing closed-loop adsorption–desorption cycles, or integrating advanced treatment methods such as distillation or electrochemical degradation to safely remove desorbed pollutants. Furthermore, the adsorption performance of phosphoric-cotton-g-GMA fibers' adsorption capabilities in real wastewater systems with numerous co-existing ions and organic substances. Investigating such competitive adsorption and potential complexation effects will

provide a more comprehensive understanding of the practical applicability and robustness of the proposed adsorbent in real environmental conditions.

ACKNOWLEDGMENTS

The authors are grateful for the support of the Institute of Tropical Forestry and Forest Products (INTROP), Universiti Putra Malaysia; the Department of Chemical and Environmental Engineering, Faculty of Engineering, Universiti Putra Malaysia (UPM); Chemistry Department, Faculty of Science, Universiti Putra Malaysia (UPM); and Malaysian Nuclear Agency for providing the research facilities. This research was funded by Universiti Putra Malaysia; Grant IPS (GP-IPS/2023/974300) with VOT NO. 9743000.

REFERENCES CITED

Aarab, N., Hsini, A., Essekri, A., Laabd, M., Lakhmiri, R., and Albourine, A. (2020). "Removal of an emerging pharmaceutical pollutant (metronidazole) using PPY-PANi copolymer: Kinetics, equilibrium and DFT identification of adsorption mechanism," *Groundwater for Sustainable Development* 11, 100416. https://doi.org/10.1016/j.gsd.2020.100416

Abbasi, A., Nasef, M. M., Babadi, F. E., Faridi-Majidi, R., Takeshi, M., Abouzari-Lotf, E., Choong, T., Somwangthanaroj, A., and Kheawhom, S. (2019). "Carbon dioxide adsorption on grafted nanofibrous adsorbents functionalized using different amines," *Frontiers in Energy Research* 7, 145. https://doi.org/10.3389/fenrg.2019.00145

Abin-Bazaine, A., Trujillo, A. C., and Olmos-Marquez, M. (2022). "Adsorption isotherms: enlightenment of the phenomenon of adsorption," in: *Wastewater Treatment* 1–15, IntechOpen. https://doi.org/10.5772/intechopen.104260

Adeyi, A. A., Bitrus, N. K., Abdullah, L. C., Popoola, L. T., Chijioke-Okere, M., Omotara, O. O., and Saber, S. E. M. (2023). "Effective sequestration of levofloxacin from wastewater by biochar-supported manganese dioxide composite: Experimental study and modelling analyses," *Environmental Engineering Research* 28(1). 210512. https://doi.org.10.4491/eer.2021.512

Agathian, K., Kannammal, L., Meenarathi, B., Kailash, S., and Anbarasan, R. (2018). "Synthesis, characterization and adsorption behavior of cotton fiber based Schiff base," *International Journal of Biological Macromolecules* 107, 1102–1112. https://doi.org/10.1016/j.ijbiomac.2017.09.086

Akhtar, J., Amin, N. A. S., and Shahzad, K. (2016). "A review on removal of pharmaceuticals from water by adsorption," *Desalination and Water Treatment*, 57 (27), 12842–12860. https://doi.org/10.1080/19443994.2015.1051121

Alnajjar, M., Hethnawi, A., Nafie, G., Hassan, A., Vitale, G., and Nassar, N. N. (2019). "Silica-alumina composite as an effective adsorbent for the removal of metformin from water," *Journal of Environmental Chemical Engineering* 7(3), 102994. https://doi.org/10.1016/j.jece.2019.102994

Aniagor, C. O., Afifi, M. A., and Hashem, A. (2022). "Rapid and efficient uptake of aqueous lead pollutant using starch-based superabsorbent hydrogel," *Polymer Bulletin* 79(8), 6373–6388. https://doi.org/10.1007/s00289-021-03817-4

Armbruster, M. H., and Austin, J. B. (1938). "The adsorption of gases on plane surfaces of mica," *Journal of the American Chemical Society* 60(2), 467–475. https://doi.org/10.1021/ja01269a066

Arnata, I. W., Suprihatin, S., Fahma, F., Richana, N., and Sunarti, T. C. (2019). "Adsorption of anionic congo red dye by using cellulose from sago frond," *Pollut. Res* 38(3), 557–567.

Bai, H., Chen, J., Zhou, X., and Hu, C. (2020). "Single and binary adsorption of dyes from aqueous solutions using functionalized microcrystalline cellulose from cotton fiber," *Korean Journal of Chemical Engineering* 37, 1926–1932. https://doi.org/10.1007/s11814-020-0621-3

Balakrishnan, A., Sillanpää, M., Jacob, M. M., and Vo, D.-V. N. (2022). "Metformin as an emerging concern in wastewater: Occurrence, analysis and treatment methods," *Environmental Research* 213, 113613.

Barsbay, M., and Güven, O. (2020). "Nanostructuring of polymers by controlling of ionizing radiation-induced free radical polymerization, copolymerization, grafting and crosslinking by RAFT mechanism," *Radiation Physics and Chemistry* 169, 107816. https://doi.org/10.1016/j.radphyschem.2018.04.009

Batool, F., Akbar, J., Iqbal, S., Noreen, S., and Bukhari, S. N. A. (2018). "Study of isothermal, kinetic, and thermodynamic parameters for adsorption of cadmium: an overview of linear and nonlinear approach and error analysis," *Bioinorganic Chemistry and Applications* 2018, 3463724. https://doi.org/10.1155/2018/3463724

Bozkaya, O., Günay, K., Arslan, M., and Gün Gök, Z. (2021). "Removal of anionic dyes with glycidyl methacrylate-grafted polyethylene terephthalate (PET) fibers modified with ethylenediamine," *Research on Chemical Intermediates*, 47 (5), 2075–2093. https://doi.org/10.1007/s11164-021-04398-7

Çavuşoğlu, F. C., Bayazit, Ş. S., Secula, M. S., and Cagnon, B. (2021). "Magnetic carbon composites as regenerable and fully recoverable adsorbents: Performance on the removal of antidiabetic agent metformin hydrochloride," *Chemical Engineering Research and Design* 168, 443–452. https://doi.org/10.1016/j.cherd.2021.01.034

Cusioli, L. F., Quesada, H. B., Castro, A. L. de B. P., Gomes, R. G., and Bergamasco, R. (2020). "Development of a new low-cost adsorbent functionalized with iron nanoparticles for removal of metformin from contaminated water," *Chemosphere* 247, 125852. https://doi.org/10.1016/j.chemosphere.2020.125852

Dave, P. N., Chopda, L. V., and Kamaliya, B. P. (2024). "Adsorption of Metformin hydrochloride and sodium diclofenac over Gum ghatti-g-poly (NIPAM-co-AA)/-o-MWCNT," *Next Materials* 4, 100190. https://doi.org/10.1016/j.nxmate.2024.100190

Ding, J., Li, X., Shan, Y., Yu, S., Yu, W., Liu, Y., Zhao, W., Li, X., Liu, M., and Ding, Y. (2021). "Super facile one-step synthesis of aromatic amine waste residue derived N-rich porous carbon for hyper efficient p-nitrophenol adsorption," *Journal of Environmental Chemical Engineering* 9(2), 105106. https://doi.org/10.1016/j.jece.2021.105106

Ferri, B. B., Wernke, G., Resende, J. F., Ribeiro, A. C., Cusioli, L. F., Bergamasco, R., and Vieira, M. F. (2024). "Natural zeolite as adsorbent for metformin removal from aqueous solutions: Adsorption and regeneration properties," *Desalination and Water Treatment* 320, 100602. https://doi.org/10.1016/j.dwt.2024.100602

Freundlich, H. (1906). "Over the adsorption in solution," *J. Phys. Chem.* 57 (May), 385–471.

Galhoum, A. A., Elshehy, E. A., Tolan, D. A., El-Nahas, A. M., Taketsugu, T., Nishikiori, K., Akashi, T., Morshedy, A. S., and Guibal, E. (2019). "Synthesis of polyaminophosphonic acid-functionalized poly(glycidyl methacrylate) for the efficient sorption of La(III) and Y(III)," *Chemical Engineering Journal*,375, 121932. https://doi.org/10.1016/j.cej.2019.121932

Han, Q., Wang, J., Goodman, B. A., Xie, J., and Liu, Z. (2020). "High adsorption of methylene blue by activated carbon prepared from phosphoric acid treated eucalyptus residue," *Powder Technology* 366, 239–248. https://doi.org/10.1016/j.powtec.2020.02.013

Hanif, Z., Tariq, M. Z., Khan, Z. A., La, M., Choi, D., and Park, S. J. (2022). "Polypyrrole-coated nanocellulose for solar steam generation: A multi-surface photothermal ink with antibacterial and antifouling properties," *Carbohydrate Polymers* 292, 119701. https://doi.org/10.1016/j.carbpol.2022.119701

Ho, Y. S., and McKay, G. (1999). "Pseudo-second order model for sorption processes," *Process Biochemistry* 34 (5), 451–465. https://doi.org/10.1016/S0032-9592(98)00112-5

Huang, X., Liu, Y., Liu, S., Li, Z., Tan, X., Ding, Y., Zeng, G., Xu, Y., Zeng, W., and Zheng, B. (2016). "Removal of metformin hydrochloride by *Alternanthera philoxeroides* biomass derived porous carbon materials treated with hydrogen peroxide," *RSC Advances* 6 (83), 79275–79284.

Hussain, S., Kamran, M., Khan, S. A., Shaheen, K., Shah, Z., Suo, H., Khan, Q., Shah, A. B., Rehman, W. U., Al-Ghamdi, Y. O., and Ghani, U. (2021). "Adsorption, kinetics and thermodynamics studies of methyl orange dye sequestration through chitosan composites films," *International Journal of Biological Macromolecules* 168, 383–394. https://doi.org/10.1016/j.ijbiomac.2020.12.054

Jawad, A. H., Mubarak, N. S. A., and Abdulhameed, A. S. (2020). "Hybrid crosslinked chitosan-epichlorohydrin/TiO2 nanocomposite for reactive Red 120 dye adsorption: kinetic, isotherm, thermodynamic, and mechanism study," *Journal of Polymers and the Environment* 28 (2), 624–637. https://doi.org/10.1007/s10924-019-01631-8

Jeong, S. K., Lee, J. S., Woo, S. H., Seo, J. A., and Min, B. R. (2015). "Characterization of anion exchange membrane containing epoxy ring and C-Cl bond quaternized by various amine groups for application in fuel cells," *Energies* 8(7), 7084–7099. https://doi.org/10.3390/en8077084

Jiang, S., Yu, T., Xia, R., Wang, X., and Gao, M. (2019). "Realization of super high adsorption capability of 2D δ-MnO2/GO through intra-particle diffusion," *Materials Chemistry and Physics* 232, 374–381. https://doi.org/10.1016/j.matchemphys.2019.05.004

Kalam, S., Abu-Khamsin, S. A., Kamal, M. S., and Patil, S. (2021). "Surfactant adsorption isotherms: A review," *ACS Omega* 6 (48), 32342–32348.

Katenta, J., Nakiguli, C., Mukasa, P., and Ntambi, E. (2020). "Removal of chromium (VI) from tannery effluent using bio-char of P*hoenix reclinata* seeds," *Green and Sustainable Chemistry* 10(3), 91-107. https://doi.org/10.4236/gsc.2020.103007

Khan, S. A., Hussain, D., and Khan, T. A. (2021). "Mechanistic evaluation of metformin drug confiscation from liquid phase on itaconic acid/kaolin hydrogel nanocomposite," *Environmental Science and Pollution Research* 28 (38), 53298–53313.

Khilchevskyi, V., and Karamushka, V. (2021). "Global water resources: distribution and demand," *Clean Water and Sanitation* 1–11. https://doi.org/10.1007/978-3-319-70061-8_101-1

Korpayev, S., Kavaklı, C., Çolak, Ş., and Kavaklı, P. A. (2018). "Preparation and characterization of ethylenediamine modified glycidyl methacrylate-grafted nonwoven cotton fabric adsorbent," *Cellulose* 25, 813–828. https://doi.org/10.1007/s10570-017-1558-5

Kumar, R., Akbarinejad, A., Jasemizad, T., Fucina, R., Travas-Sejdic, J., and Padhye, L. P. (2021). "The removal of metformin and other selected PPCPs from water by poly (3,4-ethylenedioxythiophene) photocatalyst," *Science of the Total Environment* 751, 142302. https://doi.org/10.1016/j.scitotenv.2020.142302

Li, Y., Taggart, M. A., McKenzie, C., Zhang, Z., Lu, Y., Pap, S., and Gibb, S. W. (2021). "A SPE-HPLC-MS/MS method for the simultaneous determination of prioritised pharmaceuticals and EDCs with high environmental risk potential in freshwater," *Journal of Environmental Sciences* 100, 18–27. https://doi.org/10.1016/j.jes.2020.07.013

Lin, W., Zhang, X., Li, P., Tan, Y., and Ren, Y. (2020). "Ultraviolet photolysis of metformin: mechanisms of environmental factors, identification of intermediates, and density functional theory calculations," *Environmental Science and Pollution Research* 27, 17043–17053. https://doi.org/10.1007/s11356-020-08255-9

M Saber, S. E., Abdullah, L. C., Jamil, S. N. A. M., Choong, T. S. Y., and Ting, T. M. (2021). "Trimethylamine functionalized radiation-induced grafted polyamide 6 fibers for p-nitrophenol adsorption," *Scientific Reports* 11(1), 1–17. https://doi.org/10.1038/s41598-021-97397-y

Ma, F., Gui, Y., Liu, P., Xue, Y., and Song, W. (2020). "Functional fibrous materials-based adsorbents for uranium adsorption and environmental remediation," *Chemical Engineering Journal* 390, 124597. https://doi.org/10.1016/j.cej.2020.124597

Magdy, Y. M., Altaher, H., and ElQada, E. (2018). "Removal of three nitrophenols from aqueous solutions by adsorption onto char ash: equilibrium and kinetic modeling," *Applied Water Science*, 8 (1), 26. https://doi.org/10.1007/s13201-018-0666-1

Mahmoud, M. E., El-Ghanam, A. M., Saad, S. R., and Mohamed, R. H. A. (2020). "Promoted removal of metformin hydrochloride anti-diabetic drug from water by fabricated and modified nanobiochar from artichoke leaves," *Sustainable Chemistry and Pharmacy*, 18, 100336. https://doi.org/10.1016/j.scp.2020.100336

Majd, M. M., Kordzadeh-Kermani, V., Ghalandari, V., Askari, A., and Sillanpää, M. (2022). "Adsorption isotherm models: A comprehensive and systematic review (2010−2020)," *Science of The Total Environment* 812, 151334. https://doi.org/10.1016/j.scitotenv.2021.151334

Masinga, T., Moyo, M., and Pakade, V. E. (2022). "Removal of hexavalent chromium by polyethyleneimine impregnated activated carbon: Intra-particle diffusion, kinetics and isotherms," *Journal of Materials Research and Technology* 18, 1333–1344. https://doi.org/10.1016/j.jmrt.2022.03.062

Mohamad, N. A., Abouzari Lotf, E., Mohamed, M. N., Arshad, A., and Abdullah, T. (2019). "A comparison of CO2 adsorption behaviour of mono-and diamine-functionalised adsorbents," *E3S Web of Conferences*, 1010.

Musah, M., Azeh, Y., Mathew, J. T., Umar, M. T., Abdulhamid, Z., and Muhammad, A. I. (2022). "Adsorption kinetics and isotherm models: a review," *CaJoST* 4 (1), 20–26. https:/doi.org/10.4314/cajost.v4i1.3

Niaei, H. A., and Rostamizadeh, M. (2020). "Adsorption of metformin from an aqueous solution by Fe-ZSM-5 nano-adsorbent: Isotherm, kinetic and thermodynamic

studies," *The Journal of Chemical Thermodynamics* 142, 106003. https://doi.org/10.1016/j.jct.2019.106003

Pap, S., Shearer, L., and Gibb, S. W. (2023). "Effective removal of metformin from water using an iron-biochar composite: Mechanistic studies and performance optimisation," *Journal of Environmental Chemical Engineering* 11(5), 110360. https://doi.org/10.1016/j.jece.2023.110360

Redlich, O., and Peterson, D. L. (1959). "A useful adsorption isotherm." *Journal of Physical Chemistry* 63(6), 1024. https://doi.org/10.1021/j150576a611

S. Langergren, B. K. S. (1898). "Zurtheorie der sogenannten adsorption geloesterstoffe," *Veternskapsakad Handlingar* 24, 1–39.

Saber, S. E. M., Abdullah, L. C., Ting, T. M., Jamil, S. N. A. M., Choong, T. S. Y., and Abdulkareem-Alsultan, G. (2023). "Radiation-induced grafting of glycidyl methacrylate onto natural cotton fibers and trimethylamine modification for p-nitrophenol adsorption," *Radiation Physics and Chemistry* 209, 110967. https://doi.org/10.1016/j.radphyschem.2023.110967

Saber, S. E. M., Jamil, S. N. A. M., Abdullah, L. C., Choong, T. S. Y., and Ting, T. M. (2021). "Insights into the p-nitrophenol adsorption by amidoxime-modified poly (acrylonitrile-co-acrylic acid): characterization, kinetics, isotherm, thermodynamic, regeneration and mechanism study," *RSC Advances* 11(14), 8150–8162. https://doi.org/10.1039/D0RA10910J

Samuel, S. M., Varghese, E., and Büsselberg, D. (2021). "Therapeutic potential of metformin in COVID-19: reasoning for its protective role," *Trends in Microbiology* 29(10), 894–907.

Sanchez-Silva, J. M, Collins-Martínez, V. H, Padilla-Ortega, E, Aguilar-Aguilar, A, Labrada-Delgado, G. J, Gonzalez-Ortega, O, Palestino-Escobedo, G, and Ocampo-Pérez R. (2022). "Characterization and transformation of nanche stone (*Byrsonima crassifolia*) in an activated hydrochar with high adsorption capacity towards metformin in aqueous solution," *Chemical Engineering Research and Design* 183, 580–594. https://doi.org/10.1016/j.cherd.2022.05.054

Saxena, M., Sharma, N., and Saxena, R. (2020). "Highly efficient and rapid removal of a toxic dye: adsorption kinetics, isotherm, and mechanism studies on functionalized multiwalled carbon nanotubes," *Surfaces and Interfaces* 21, 100639. https://doi.org/10.1016/j.surfin.2020.100639

Scheurer, M., Michel, A., Brauch, H. J., Ruck, W., and Sacher, F. (2012). "Occurrence and fate of the antidiabetic drug metformin and its metabolite guanylurea in the environment and during drinking water treatment," *Water Research* 46(15), 4790–4802.

Schneider, C. A., Rasband, W. S., and Eliceiri, K. W. (2012). "NIH Image to ImageJ: 25 years of image analysis," *Nature Methods* 9(7), 671–675. https://doi.org/10.1038/nmeth.2089

Tahir, M., Raza, A., Nasir, A., and Yasin, T. (2021). "Radiation induced graft polymerization of glycidyl methacrylate onto sepiolite," *Radiation Physics and Chemistry*, 179, 109259. https://doi.org/10.1016/j.radphyschem.2020.109259

Ting, M., Nasef, Ee and Ling A. W. (2019). "Kinetics of radiation grafting of glycidyl methacrylate and vinylbenzyl chloride onto polymer fibers," *Journal of Engineering Science and Technology* 14(2), 646–658.

Vinet, L., and Zhedanov, A. (2011). "A 'missing' family of classical orthogonal polynomials," *Journal of Physics A: Mathematical and Theoretical* 44(8), 327–356. https://doi.org/10.1088/1751-8113/44/8/085201

Wang, and Guo X. (2020). "Adsorption kinetic models: Physical meanings, applications, and solving methods," *Journal of Hazardous Materials* 390, 122156. https://doi.org/10.1016/j.jhazmat.2020.122156

Weber, W. J., and Morris, J. C. (1963). "Closure to 'Kinetics of Adsorption on carbon from solution," *Journal of the Sanitary Engineering Division* 89(6), 53–55. https://doi.org/10.1061/jsedai.0000467

Weber, W. J., and Smith, E. H. (1987). "Simulation and design models for adsorption processes," *Environmental Science and Technology* 21(11), 1040–1050. https://doi.org/10.1021/es00164a002

WHO (2019). "World health organization model list of essential medicines," *Mental and Holistic Health: Some International Perspectives*, 119–134

Yang, J., Liang, T., Pan, B., Xu, X., Guo, Y., Shi, W., Long, Q., Deng, J., Yao, Q., and Wang, Z. (2024). "A spherical adsorbent produced from a bagasse biochar chitosan assembly for selective adsorption of platinum-group metals from wastewater," *International Journal of Biological Macromolecules* 266, 131142. Elsevier.

Zhan, Y., Zhao, S., Wan, X., and He, S. (2019). "Hierarchical Fe_3O_4-derived organic/inorganic hybrids constructed by modified bio-inspired functionalization: efficient adsorbents for water-soluble methylene blue and mechanism," *Journal of Chemical Technology and Biotechnology* 94(5), 1638–1650.

Article submitted: July 20, 2025; Peer review completed: October 25, 2025; Revised version received and accepted: January 12, 2026; Published: January 26, 2026.
DOI: 10.15376/biores.21.1.2283-2314